Analytical & Bioanalytical Chemistry

Metabolism of the new psychoactive substances N,N-diallyltryptamine (DALT) and 5-methoxy-DALT and their detectability in urine by GC-MS, LC-MSn, and LC-HR-MS/MS

Journal:	*Analytical and Bioanalytical Chemistry*
Manuscript ID:	ABC-01148-2015.R1
Type of Paper:	Research Paper
Date Submitted by the Author:	n/a
Complete List of Authors:	Michely, Julian; Saarland University, Dept. of Experimental & Clinical Toxicology Helfer, Andreas; Saarland University, Dept. of Experimental & Clinical Toxicology BRANDT, SIMON Meyer, Markus; Karolinska Institutet, Maurer, Hans; Saarland University, Department of Experimental and Clinical Toxicology
Keywords:	Bioanalytical methods, Biological samples, Drug monitoring / Drug screening, Forensics / Toxicology, Mass spectrometry / ICP-MS

Metabolism of the new psychoactive substances *N,N*-diallyltryptamine (DALT) and 5-methoxy-DALT and their detectability in urine by GC-MS, LC-MS^n, and LC-HR-MS/MS

Julian A. Michely * Andreas G. Helfer * Simon D. Brandt * Markus R. Meyer * Hans H. Maurer

J. A. Michely * A. G. Helfer * M. R. Meyer * H. H. Maurer (corresponding author)

Department of Experimental and Clinical Toxicology, Institute of Experimental and Clinical Pharmacology and Toxicology, Saarland University, 66421 Homburg (Saar), Germany

e-mail: hans.maurer@uks.eu

Telephone: +49 – 6841 16 26050

Fax: +49 – 68941 16 26051

Simon D. Brandt

School of Pharmacy and Biomolecular Sciences, Liverpool John Moores University, L3 3AF, Liverpool, United Kingdom

Markus R. Meyer

Present address: Farmakologiska laboratoriet, Klinisk farmakologi, Karolinska Universitetssjukhuset Huddinge, Karolinska Institutet, 141 86 Stockholm, Sweden

Abstract

N,N-Diallyltryptamine (DALT) and 5-methoxy-DALT (5-MeO-DALT) are synthetic tryptamine derivatives that are commonly referred to the so-called new psychoactive substances (NPS). They show psychoactive effects similar that may be similar to other tryptamine derivatives. The aims of the present work were to study the metabolic fate and detectability in urine after intake of DALT and 5-MeO-DALT. For metabolism studies, rat urine samples obtained following high dose administration were prepared by precipitation and analyzed by liquid chromatography-high resolution-mass spectrometry (LC-HR-MS/MS). According to the identified metabolites, multiple aromatic and aliphatic hydroxylations, *N*-dealkylation, *N*-oxidation, and combinations thereof could be proposed as main metabolic pathways for both compounds. *O*-Demethylation was additionally found for 5-MeO-DALT and extensive glucuronidation or sulfation for both compounds after phase I transformation. The cytochrome P450 (CYP) isoenzymes predominantly involved in DALT metabolism were CYP2C19, CYP2D6, and CYP3A4 and those mainly involved in 5-MeO-DALT metabolism were CYP1A2, CYP2C19, CYP2D6, and CYP3A4, respectively. For the detectability studies, rat urine samples were screened by the authors' GC-MS, LC-MS^n, and LC-HR-MS/MS urine screening approaches following administration of low doses. The LC-MS^n and LC-HR-MS/MS approaches were deemed suitable for monitoring consumption of both compounds. The most abundant targets were a ring hydroxy metabolite of DALT or the *N,O*-bis-dealkyl metabolite of 5-MeO-DALT as well as their glucuronides. The GC-MS approach only allowed for the screening of DALT via its main metabolites.

Keywords designer drugs; DALT; 5-MeO-DALT; metabolism; SUSA; LC-HR-MS/MS

Introduction

Synthetic tryptamines belong to one class of new psychoactive substances (NPS) in addition to synthetic cannabinoids, phenethylamines, synthetic cathinones, and others [1, 2]. They interact with the serotonergic system, which includes activation of the 5-HT_{1A} and 5-HT_{2A} receptor subtypes [3] and increase of serotonin release [4-8]. Active oral dosage levels of *N,N*-diallyltryptamine (DALT) and 5-methoxy-DALT (5-MeO-DALT) have been suggested to range from above 40 mg for DALT and 12-20 mg for 5-MeO-DALT, respectively [9-11]. Their chemical structures are depicted in Fig. 1. The control status of both substances differs across the globe. Misuse of 5-MeO-DALT and the association with adverse effects has been recently reported [12, 13], which serves as a reminder that the ability to carry out suitable toxicological analysis is urgently needed. As far as DALT is concerned, no corresponding data are available.

Analytical methods used for the characterization of *N,N*-dialkylated tryptamines [14] and naturally-occurring *N,N*-dimethylated tryptamines found in psychoactive beverages [15] have been reviewed but without reference to determination in biofluids. Information on metabolism in urine is important so that appropriate targets can be identified. Katagi et al. reviewed the general metabolic steps and toxicologic analysis of a number of selected 5-methoxy-*N,N*-dialkyltryptamines [16]. Metabolism and detectability of DALT and 5-MeO-DALT in relevant matrices have not yet been described. Therefore, the aim of the present work was to identify phase I and II metabolites of DALT and 5-MeO-DALT in rat urine as well as in pooled human liver microsomes (pHLM) by liquid chromatography (LC)-high resolution (HR)-MS/MS and to identify the human cytochrome-P450 (CYP) isoenzymes involved in the main metabolic steps. Furthermore, the detectability of DALT and 5-MeO-DALT in urine by the authors' urine screening approaches (SUSA) using GC-MS, LC-MS^n, or LC-HR-MS/MS was tested.

Experimental

Chemicals and reagents

DALT, DALT-d_4, and 5-MeO-DALT were synthesized following established methods [17], isocitrate and isocitrate dehydrogenase from Sigma (Taufkirchen, Germany), $NADP^+$ from Biomol (Hamburg, Germany), acetonitrile (LC-MS grade), ammonium formate (analytical grade), formic acid (LC-MS grade), methanol (LC-MS grade), and all other chemicals and biochemicals from VWR (Darmstadt, Germany). The baculovirus-infected insect cell microsomes (Supersomes) containing 1 nmol/mL of human cDNA-expressed CYP1A2, CYP2A6, CYP2B6, CYP2C8, CYP2C9, CYP2C19, CYP2D6, CYP2E1 (2 nmol/mL), CYP3A4, or CYP3A5 (2 nmol/mL), and pooled human liver microsomes (pHLM, 20 mg microsomal protein/mL, 400 pmol total CYP/mg protein) were obtained from BD Biosciences (Heidelberg, Germany). After delivery, the microsomes were thawed at 37 °C, divided into aliquots, snap-frozen in liquid nitrogen, and stored at -80 °C until use.

Urine samples

As usual, investigations were performed using rat urine samples from male Wistar rats (Charles River, Sulzfeld, Germany) for toxicological diagnostic reasons. The compound was administered once in an aqueous suspension by gastric intubation in a single 20 mg/kg body mass (BM) dose for the identification of the metabolites and once in a single 1 mg/kg BM dose for toxicological analysis.

The rats were housed in metabolism cages for 24 h, having water ad libitum. Urine was collected separately from feces over a 24 h period. Blank urine samples were collected before drug administration to confirm the absence of interfering compounds. The samples were directly analyzed and then stored at -20 °C.

Sample preparation for identification of phase I and II metabolites by LC-HR-MS/MS

As described previously [18], 500 µL of acetonitrile was added to 100 µL of urine. The mixture was shaken on a rotary shaker for 2 min. After centrifugation for 2 min at 10,000×*g*, 500 µL was transferred into a glass vial and evaporated to dryness under a gentle stream of nitrogen at 70 °C. The residue was dissolved in 50 µL of methanol. A 10-µL aliquot of each extract was then injected onto the LC-HR-MS/MS system.

Microsomal incubations for pHLM and initial CYP activity screening studies

Conditions for the performance of the microsomal incubations for each isomer were published previously [19]. Briefly, drugs (50 µmol/L each) were incubated with the CYP isoenzymes (50 pmol/mL, each) CYP1A2, CYP2A6, CYP2B6, CYP2C8, CYP2C9, CYP2C19, CYP2D6, CYP2E1, CYP3A4, CYP3A5, or pHLM (1 mg protein/mL) for 30 min. Reactions were initiated by addition of the substrate and stopped with 50 µL of ice-cold acetonitrile containing DALT-d_4 (1 mg/L) as internal standard. The solution was centrifuged for 2 min at 14,000×*g*, 50 µL of the supernatant phase were transferred to a glass vial and a 10-µL aliquot injected onto the LC-HR-MS/MS system.

LC-HR-MS/MS apparatus for identification of phase I and II metabolites in urine and microsomal incubations

According to published procedures [20], the extracts were analyzed using a Accela LC system consisting of an HTC PAL autosampler, a degasser, two 1250 quaternary pumps, an Aria Transcend TLX-I HTLC system, and a valve interface module with built-in switching valves, all controlled by the Aria software version 1.6.3, coupled to a Q-Exactive system equipped with a heated electrospray ionization (HESI)-II source and Xcalibur 2.2 SP1.48 software (all of ThermoFisher, Dreieich,

Germany). Mass calibration was done according to the manufacturer's recommendations every 72 h using external mass calibration. According to Helfer et al. (submitted for publication), the LC conditions were as follows: a ThermoFisher Accucore PhenylHexyl column (100 mm × 2.1 mm I.D., 2.6 µm), guarded by an UHP filter cart (0.5 µm). Chromatography was performed at 35 °C maintained by an analytical column heater (HotDog 5090, Prolab, Reinach, Switzerland). The mobile phases consisted of 2 mM aqueous ammonium formate plus 0.1% formic acid (pH 3, eluent A) and 2 mM aqueous ammonium formate with acetonitrile:methanol (50:50, v/v; 1% water) plus 0.1% formic acid (eluent B). The flow rate was set to 0.5 mL/min for 10 min and 0.8 mL/min from 10-13.5 min. The gradient was programmed as follows: 0-1.0 min 99% A, 1-10 min to 1% A, 10-11.5 min hold 1% A, 11.5 - 13.5 min hold 99% A. The HESI-II source conditions were as follows: heater temperature, 320 °C; sheath gas, 60 arbitrary units (AU); auxiliary gas, 10 AU; spray voltage, 3.00 kV; capillary temperature, 320 °C; and S-lens RF level, 60.0. Mass spectrometry was performed in positive ionization mode using full scan mode and a subsequent data-dependent acquisition (DDA) mode. The settings for the full scan mode were as follows: scan range, *m/z* 130-1000; resolution, 35,000; microscans, 1; automatic gain control (AGC) target, 1e6; and maximum injection time (IT), 120 ms. The settings for the DDA mode were as follows: resolution, 17,500; microscans, 1; AGC target, 2e5; maximum IT, 250 ms; loop count, 5; isolation window, *m/z* 1.0; high collision dissociation (HCD) cell stepped normalized collision energy (NCE), 17.5, 35, and 52.5%; spectrum data type, profile; intensity threshold, 4.0e3; dynamic exclusion, 8.0 s.

GC-MS SUSA

According to published procedures [21], the urine sample (5 mL) was divided into two aliquots where one part was submitted to acid hydrolysis followed by extraction of the combined parts with a dichloromethane-isopropanol-ethyl acetate mixture. After evaporation, the residue was acetylated with an acetic anhydride-pyridine mixture under microwave irradiation, again evaporated and

reconstituted in 100 µL of methanol. A 1-µL aliquot was injected onto the GC-MS system. This consisted of a Hewlett Packard (HP, Agilent, Waldbronn, Germany) 5890 Series II gas chromatograph combined with an HP 5972A MSD mass spectrometer and an HP MS ChemStation (DOS series) with HP G1034C software version C03.00. The GC conditions were as follows: splitless injection mode; column, ThermoFisher TG-1MS capillary (12 m x 0.2 mm I.D.); cross-linked methyl silicone, 330 nm film thickness; injection port temperature, 280 °C; carrier gas, helium; flow rate, 1 mL/min; column temperature, programmed from 100 to 310 °C at 30 °C/min; initial time, 2 min; final time, 5 min. The MS conditions were as follows: full scan mode, *m/z* 50-550; electron ionization (EI) mode, ionization energy, 70 eV; ion source temperature, 220 °C; and capillary direct interface, 280 °C [22].

The full scan data files were evaluated by the automated mass spectral deconvolution and identification system (AMDIS) (http://chemdata.nist.gov/mass-spc/amdis/) in simple mode. The target library was a modified version of the Maurer/Pfleger/Weber MPW_2015 library [23]. The deconvolution parameter settings were as follows [24]: width, 32; adjacent peak subtraction, 2; resolution, high; sensitivity, very high; shape requirements, low; minimum match factor, 50.

LC-MS^n SUSA

The workup was identical to the procedure described above for identification of phase I and II metabolites. Analysis was performed using a LXQ linear ion trap MS equipped with an HESI II source and coupled to an Accela LC system (all from ThermoFisher). The LC and the MS settings were described elsewhere [18]. Briefly, DDA was conducted on precursor ions selected from MS^1: MS^1 was performed in the full scan mode (*m/z* 100-800) and MS^2 and MS^3 were performed in the DDA mode. ThermoFisher Xcalibur 2.2 SP1.48 software was used for data acquisition, NIST MS Search 2.0 (National Institute of Standards and Technology, Gaithersburg, MD, USA) for library generation, ThermoFisher ToxID 2.1.1 for automatic target screening in the MS^2 screening mode.

The settings were as follows: retention time (RT) window, 20 min; RT, 0.1 min; signal threshold, 100; search index, 600; and reverse search index, 700. ToxID was run automatically after file acquisition using a Xcalibur processing method starting the software tool. The target library was a modified version of the Maurer/Wissenbach/Weber MWW_2014 library [25].

LC-HR-MS/MS SUSA

The workup and the LC-HR-MS/MS method were the same as described above for identification of phase I and II metabolites. ThermoFisher TraceFinder Clinical Research 3.2 software was used for data evaluation as described by Helfer et al. (submitted for publication).

Results and discussion

Identification of the phase I and phase II metabolites by LC-HR-MS/MS

The structures of the urinary metabolites were deduced from their MS/MS spectra in correlation to the spectra of the parent compounds. The fragmentation patterns were postulated based on established rules [26]. The LC-HR-MS/MS spectra of DALT and its phase I metabolites are given in Fig. S1, those of 5-MeO-DALT and its phase I metabolites in Fig. S2 supplied as electronic supplementary material. The LC-HR-MS/MS spectra of the phase II metabolites of DALT are given in Fig. S3 and those of 5-MeO-DALT in Fig. S4, respectively. In addition, the proposed chemical structures, accurate masses of the ions, calculated elemental formulas, and mass error values in parts per million (ppm) are given in the corresponding spectra.

Proposed fragmentation patterns for identification of the phase I metabolites by LC-HR-MS/MS

For better description of positions, the basic structure was divided into three sections (Fig. 1), the aromatic ring (section 1), the ethyl spacer (section 2), and *N*,*N*-diallylamine (section 3). In the following, important fragmentation patterns of the mass spectra of DALT, 5-MeO-DALT, and their phase I metabolites will be discussed in detail. All masses within this paragraph are the calculated, exact masses.

DALT

The spectrum of the parent compound is given in Fig. S1, no. 1. In addition to the protonated molecule with *m/z* 241.1699 ($C_{16}H_{21}N_2^+$), the DALT spectrum showed a characteristic fragment ion with *m/z* 144.0808 ($C_{10}H_{10}N^+$) representing the ethyl indole residue (section 1+2), a fragment ion with *m/z* 117.0701 ($C_9H_9^+$) representing the indole ring after loss of HCN, and *m/z* 110.0964 ($C_7H_{12}N^+$) that represented the *N*,*N*-diallylmethanimine residue (section 3) following typical α-cleavage [14].

When section 3 in the metabolites was unchanged, fragment ions could be observed with *m/z* 110.0964 (nos. 5, 7-13 in Fig. S1) and if *N*-deallylated (- 40.0313 u) with *m/z* 70.0651 (2-4 in Fig. S1). When sections 1 and 2 were unmodified, fragment ions with *m/z* 144.0808 (2, 12 in Fig. S1) appeared, when mono-hydroxylated (+ 15.9949 u) with *m/z* 160.0757 (3-5, 7, 8, 11 in Fig. S1), when di-hydroxylated (+ 31.9898 u) with *m/z* 176.0706 (9, 10 in Fig. S1), or when tri-hydroxylated (+ 47.9847 u) with *m/z* 192.0655 (13 in Fig. S1). Furthermore, fragment ions with *m/z* 117.0699 (2-6, 12 in Fig. S1) were observed in *N*-deallylated metabolites or in those with an unchanged indole ring. In case of ring mono-hydroxylation, ions with *m/z* 115.0542 ($C_9H_7^+$) were formed instead (3, 4, 7, 8 in Fig. S1), representing the hydroxylated indole ring after loss of HCN and further elimination of water. Both fragments were not formed in compounds with multiple hydroxylation sites on the ring system or hydroxylations in section 2. Minor fragment ions with *m/z* 132.0808 ($C_9H_{10}N^+$) representing methyl indole residues were formed by all compounds with either an un-substituted or mono-hydroxylated indole ring (2-5, 7, 8, 11 in Fig. S1).

The two hydroxy metabolites (7, 8 in Fig. S1) showed protonated molecule with *m/z* 257.1648 ($C_{16}H_{21}ON_2^+$) and identical fragments. Besides fragment ion with *m/z* 160.0757 ($C_{10}H_{10}ON^+$), no loss of water (- 18.0100 u) could be observed indicating hydroxylation in section 1. The spectra of the four di-hydroxy metabolites (9-12 in Fig. S1) showed the protonated molecule with *m/z* 273.1598 ($C_{16}H_{21}O_2N_2^+$). Three of them (9-11 in Fig. S1) showed a fragment ion with *m/z* 231.1128 ($C_{13}H_{15}O_2N_2^+$) resulting from allyl cleavage (see also fragment ion with *m/z* 261.1234 in spectra nos. 16 and 17 in Fig. S2). Two isomers (9, 10 in Fig. S1) showed an additional fragment ion with *m/z* 148.0393 ($C_8H_6O_2N^+$) indicating that two hydroxylations occurred in section 1. The third isomer (11 in Fig. S1) showed a loss of two hydrogens (- 2.0156 u) to give *m/z* 174.0550 ($C_{10}H_8O_2N^+$) instead of a fragment ion with *m/z* 176.0706 ($C_{10}H_{10}O_2N^+$) representing the same structure with a double bond in section 2. A further loss of carbon monoxide (- 27.9950 u) could be observed leading to *m/z* 146.0600 ($C_9H_8ON^+$). The presence of the fragment ion with *m/z* 110.0964 ($C_7H_{12}N^+$) suggested the formation of one aryl hydroxy group in section 1 and one alkyl hydroxy group in section 2. The fourth isomeric spectrum (12 in Fig. S1) showed different fragmentation patterns. The main fragment ion with *m/z* 144.0808 ($C_{10}H_{10}N^+$) and *m/z* 142.0863 ($C_7H_{12}O_2N^+$) indicated that both oxygens were introduced at the *N,N*-diallylic group in section 3 leaving section 1 and 2 unmodified. Instead of a fragment ion with *m/z* 231.1128 (9-11 in Fig. S1), a shift of one hydrogen (+ 1.0078 u) was observed to give a radical cation with *m/z* 232.1206 ($C_{13}H_{16}O_2N_2^{+\bullet}$). Despite the shift, this fragment ion allowed for the positions of the hydroxy groups to be established. Either both were located at the same allyl group or one hydroxy was located at the nitrogen forming an *N*-oxide. Beyond this, the fragment ion with *m/z* 100.0757 ($C_5H_{10}ON^+$) represented a hydroxylated *N*-allyl-*N,N*-bis-methyl amine with two possible positions. Either one oxidation led to an *N*-oxide or both hydroxy groups were located at different substituents, although this might be excluded from detection of the fragment ion with *m/z* 232.1206. Thus, the proposed metabolite structure seemed more consistent with an *N*-oxide. In general, *N*-oxides were eluting later on reversed phase columns compared to the parent compounds. A corresponding metabolite representing allylic hydroxylation in

section 3 was not detected. As far as the detected hydroxy and di-hydroxy metabolites were concerned (7-12 in Fig. S1), the proposed *N*-oxide had the longest RT (4.5 min) compared to all others (RT between 3.4 and 4.3 min), which appear to support this suggestion. Among hydroxy and di-hydroxy metabolites, tri-hydroxy metabolite could also be identified (13 in Fig. S1). The mass spectrum showed a protonated molecule with *m/z* 289.1547 ($C_{16}H_{21}O_3N_2^+$) and a fragment ion with *m/z* 164.0342 ($C_8H_6O_3N^+$) that corresponded to addition of one oxygen (+ 15.9949 u) in contrast to the fragment ion with *m/z* 148.0393 ($C_8H_6O_2N^+$) observed in aryl di-hydroxy metabolites. It represented the threefold aryl hydroxylated metabolite.

Protonated molecules with *m/z* 255.1492 ($C_{16}H_{19}ON_2^+$) revealed two oxo metabolites (5, 6 in Fig. S1). The first isomer spectrum (5 in Fig. S1) showed fragment ion analogous to the aryl hydroxy metabolites (7, 8 in Fig. S1). However, instead of *m/z* 115.0542 ($C_9H_7^+$), a fragment ion with *m/z* 117.0699 ($C_9H_9^+$) was detected that pointed toward an un-substituted indole ring as described above. Regarding these fragments, the proposed keto function could only be positioned in section 2. The second isomer spectrum (6 in Fig. S1) showed completely different fragmentation patterns compared to all other spectra. Both main fragment ion with *m/z* 214.1101 ($C_{13}H_{14}ON_2^{+\bullet}$) and *m/z* 173.0709 ($C_{10}H_9ON_2^+$) contained the unchanged amine group and calculated chemical formulas could only be explained by ring closure with a suggested structure given in spectrum 6 in Fig. S1. The initial step may reflect hydroxylation in the amine α-position representing a rather instable hemiaminal. This chemical structure could either degrade, oxidized to an amide, or could engage in nucleophilic attack of the indole 2-position position. The product after ring closure could explain both main fragment ion after loss of the allyl groups (- 41.0391 u), respectively, as well as *m/z* 146.0600 ($C_9H_8ON^+$) after further loss of hydrocyanic acid (- 27.0109 u).

A metabolic *N*-dealkylation step led to a spectrum (2 in Fig. S1) that revealed a protonated molecule with *m/z* 201.1386 ($C_{13}H_{17}N_2^+$) and a typical fragment ion with *m/z* 70.0651 ($C_4H_8N^+$) similar to what was described above. Combinations with mono-hydroxylation led to two isomers (3, 4 in Fig. S1) with protonated molecule with *m/z* 217.1335 ($C_{13}H_{17}ON_2^+$). Both isomers showed

similar fragmentation patterns as aryl hydroxy metabolites (7, 8 in Fig. S1), except for the allyl shift and an additional fragment ion with *m/z* 148.0757 ($C_9H_{10}ON^+$), which represented aryl hydroxylation in a methylindole species. It should be mentioned that this fragment ion differed from fragment ion with *m/z* 148.0393 ($C_8H_6O_2N^+$) detected in aryl di-hydroxy metabolites (9, 10 in Fig. S1).

5-MeO-DALT

The 5-MeO-DALT spectrum is given in Fig. S2, no. 1. Basic fragmentation patterns were analogous to those of DALT. Thus, in addition to the protonated molecule with *m/z* 271.1805 ($C_{17}H_{23}ON_2^+$), the ethyl indole residue (section 1+2) was represented by fragment ion with *m/z* 174.0913 ($C_{11}H_{12}ON^+$), the indole ring after HCN loss by fragment ion with *m/z* 117.0699 ($C_9H_9^+$), and the iminium ion (section 3) by fragment ion with *m/z* 110.0964 ($C_7H_{12}N^+$). Moreover, an additional fragment ion was observed with *m/z* 159.0679 ($C_{10}H_9ON^+$) representing the hydroxy ethylindole part following radical loss of a methyl group (see also spectra nos. 3, 18, 21 in Fig. S2).

When section 3 in the metabolites was unmodified, fragment ions could be observed with *m/z* 110.0964 (7-11, 13-17, 19, 20 in Fig. S2) and when *N*-deallylated (- 40.0313 u), ions with *m/z* 70.0651 (2-6 in Fig. S2) were detected. When there was no metabolic change in sections 1 and 2, fragment ion with *m/z* 174.0913 (3, 18, 21 in Fig. S2) appeared, when mono-hydroxylated with *m/z* 190.0863 (5, 6, 10, 11, 13, 14 in Fig. S2), when di-hydroxylated with *m/z* 206.0812 (16, 17 in Fig. S2), when tri-hydroxylated with *m/z* 222.0761 (20 in Fig. S2), or when *O*-demethylated with *m/z* 160.0757 (2 in Fig. S2), respectively. *O*-Demethylation in combination with mono-hydroxylation led to fragment ion with *m/z* 176.0706 (4, 8 in Fig. S2) or, when di-hydroxylation was involved, to a fragment ion with *m/z* 192.0655 (15 in Fig. S2). Again, the fragmented indole ring was represented by fragment ion with *m/z* 117.0699 (2, 3, 10-12 in Fig. S2) or 115.0542 (2, 7 in Fig. S2). Both fragments were not formed in compounds with multiple hydroxylations at the ring system, with hydroxylations in section 2 (4, 5, 8, 9, 13, 15-21 in Fig. S2), or with aryl-hydroxy-methoxy substituents (6, 14 in Fig.

S2). Finally, the methyl indole residues were represented by fragment ion with *m/z* 132.0808 ($C_9H_{10}N^+$) in all compounds that either displayed an un-substituted or mono-hydroxylated indole ring (2, 7 in Fig. S2), except for those hydroxylated in section 2 (9 in Fig. S2).

The two hydroxy metabolites (13, 14 in Fig. S2) showed a protonated molecule with *m/z* 287.1754 ($C_{17}H_{23}O_2N_2^+$). The first isomer (13 in Fig. S2) showed metabolic hydroxylation in section 2, identified by a fragment ion with *m/z* 158.0600 ($C_{10}H_8ON^+$) representing the hydroxy ethylene indole part after subsequent loss of the *O*-methyl group and water. For the second isomer (14 in Fig. S2), a fragment ion with *m/z* 162.0550 ($C_9H_8O_2N^+$) represented the di-hydroxy methyl indole part after loss of the *O*-methyl group, which specified the position of hydroxylation in section 1. Three di-hydroxy metabolites were detected (16-18 in Fig. S2) with protonated molecules with *m/z* 303.1703 ($C_{17}H_{23}O_3N_2^+$). Two of them (16, 17 in Fig. S2) were consistent with aryl di-hydroxy metabolites with fragment ion with *m/z* 178.0499 ($C_9H_8O_3N^+$: 162.0550 + 15.9949 u) as described above. In contrast, the third isomer (18 in Fig. S2) showed a fragment ion with *m/z* 174.0913 ($C_{11}H_{12}ON^+$) indicating a loss of both hydroxy groups within section 3. This could be confirmed by the detection of ion with *m/z* 142.0863 ($C_7H_{12}O_2N^+$: 110.0964 + 31.9899 u). Furthermore, the fragment ion with *m/z* 100.0757 ($C_5H_{10}ON^+$) represented hydroxylated *N*-allyl-*N*,*N*-bis-methyl amine, as already described for DALT, and again two options could be considered. Either the two hydroxy groups were located at different *N*-allyl positions or one of them was an *N*-oxide. Considering *N*-oxidation, a comparable fragmentation pattern as for the proposed DALT *N*-oxide and a comparable shift in RT (4.4 min) compared to other metabolites could be observed, again suggesting the presence of the *N*-oxide. Three tri-hydroxy metabolites (19-21 in Fig. S2) were found with protonated molecules with *m/z* 319.1652 ($C_{17}H_{23}O_4N_2^+$). Isomer one (19 in Fig. S2) showed only two fragment ions with *m/z* 110.0964 ($C_7H_{12}N^+$) and 178.0499 ($C_9H_8O_3N^+$). The first fragment ion represented a non-hydroxylated section 3, the second fragment ion a tri-hydroxy methylindole after loss of the *O*-methyl group as already described above. Both fragment ions indicated the positions of two aryl hydroxy groups presented in section 1 and one in section 2. In isomer two (20 in Fig. S2), all

hydroxy groups were positioned in section 1, confirmed by detection of a fragment ion with *m/z* 194.0448 ($C_9H_8O_4N^+$) representing threefold hydroxylated methyl indole. Isomer three (21 in Fig. S2) exhibited all hydroxy groups on the alkyl side chain in section 3. Confirmation of this assignment came from a fragment ion with *m/z* 174.0913 ($C_{11}H_{12}ON^+$) as described for the spectrum of the parent compound and a fragment ion with *m/z* 158.0812 ($C_7H_{12}O_3N^+$: 110.0964 + 47.9848 u). Regarding fragmentation patterns and RT (4.4 min), the presence of an *N*-oxide was indicated.

Three oxo metabolites showed protonated molecules with *m/z* 285.1598 ($C_{17}H_{21}O_2N_2^+$) (10-12 in Fig. S2). According to their common fragmentation patterns, the oxygen positions were consistent with section 2 for two of the isomers (10, 11 in Fig. S2) as proven by the presence of fragment ion with *m/z* 110.0964 ($C_7H_{12}N^+$) and the loss of carbon monoxide (- 27.9950 u) in fragment ions with *m/z* 190.0863 ($C_{11}H_{12}O_2N^+$) to result in formation of *m/z* 162.0913 ($C_{10}H_{12}ON^+$). It should be mentioned that this fragment ion differed from the fragment ion with *m/z* 162.0550 ($C_9H_8O_2N^+$) representing di-hydroxy methylindole regarding loss of the *O*-methyl group as described above (14, 16, 17 in Fig. S2). The third isomer (12 in Fig. S2) showed fragmentation patterns similar to those described for DALT in spectrum no. 6 in Fig. S1. Fragment ions with *m/z* 244.1206 ($C_{14}H_{16}O_2N_2^{+\bullet}$), 203.0815 ($C_{11}H_{11}O_2N_2^+$), and 176.0706 ($C_{10}H_{10}O_2N^+$) were considered analogous to fragment ions with *m/z* 214.1101 ($C_{13}H_{14}ON_2^{+\bullet}$), 173.0709 ($C_{10}H_9ON_2^+$), and 146.0600 ($C_9H_8ON^+$), respectively.

N-Dealkylation led to a spectrum (3 in Fig. S2) that showed a protonated molecule with *m/z* 231.1492 ($C_{14}H_{19}ON_2^+$) and a typical fragment ion with *m/z* 70.0651 ($C_4H_8N^+$) as already described above. Combinations of *N*-dealkylation and hydroxylation led to two metabolites with protonated molecule with *m/z* 247.1441 ($C_{14}H_{19}O_2N_2^+$) (5, 6 in Fig. S2) and a fragment ion with *m/z* 178.0863 ($C_{10}H_{12}O_2N^+$). This was degraded either to give a fragment ion with *m/z* 158.0600 ($C_{10}H_8ON^+$), indicating hydroxylation in section 2, or to a fragment ion with *m/z* 162.0550 ($C_9H_8O_2N^+$), indicating an aryl hydroxylation in section 1.

O-Demethylation (7 in Fig. S2) led to a protonated molecule with *m/z* 257.1648 ($C_{16}H_{21}ON_2^+$) with fragment ions similar to those described for aryl hydroxy DALT (7, 8 in Fig. S1). Two

O-demethyl hydroxy metabolites could be postulated (8, 9 in Fig. S2) with protonated molecules with *m/z* 273.1598 ($C_{16}H_{21}O_2N_2^+$). Fragmentation of the first isomer (8 in Fig. S2) did not differ from that obtained from aryl di-hydroxy DALT (9, 10 in Fig. S1) with fragment ions with *m/z* 162.0550 ($C_9H_8O_2N^+$) and hydroxylation in section 1. For the second isomer (9 in Fig. S2), a loss of water (-18.0100 u) from fragment ion with *m/z* 176.0706 ($C_{10}H_{10}O_2N^+$) to *m/z* 158.0606 ($C_{10}H_8ON^+$) indicated hydroxylation in section 2. An *O*-demethyl di-hydroxy metabolite (15 in Fig. S2) could be detected with a protonated molecule with *m/z* 289.1547 ($C_{16}H_{21}O_3N_2^+$) and fragment ions similar to those identified for aryl tri-hydroxy DALT (13 in Fig. S1). Thus, the two metabolically formed hydroxy groups were located in section 1. The spectrum of the *O*-demethyl *N*-dealkyl metabolite (2 in Fig. S2) showed a protonated molecule with *m/z* 217.1335 ($C_{13}H_{17}ON_2^+$) and fragment ions that did not differ from those of *N*-dealkyl aryl hydroxy DALT (3, 4 in Fig. S1). Further hydroxylation of this metabolite (4 in Fig. S2) led to a protonated molecule with *m/z* 233.1285 ($C_{13}H_{17}O_2N_2^+$). The position of the hydroxy group was thought to be located in section 2 because of the observed fragment ion with *m/z* 148.0757 ($C_9H_{10}ON^+$) that excluded the position of the second hydroxy group on the methylindole ring.

Proposed fragmentation patterns for identification of the phase II metabolites by LC-HR-MS/MS

In the following, important fragmentation patterns of the mass spectra of DALT, 5-MeO-DALT phase II metabolites will be discussed. All masses within the paragraph are the calculated exact masses.

DALT

In general, the conjugates of the aryl mono-hydroxy metabolites showed same fragment ion as the underlying phase I metabolites, following conjugate losses of -79.9568 u for sulfates or -176.0321 u for glucuronides, with additional fragment ions with *m/z* 240.0325 (3S, 4S, 7S, 8S in Fig. S3) for

sulfates or at 336.1078 (3G, 4G, 7G, 8G in Fig. S3) for glucuronides. These fragment ions represented the ethyl indole part (sections 1+2) with + 79.9568 u for sulfates or + 176.0321 u for glucuronides. In total, sulfates and glucuronides could be detected for two aryl hydroxy isomers (7S, 8S, 7G, 8G in Fig. S3) and two *N*-dealkyl aryl-hydroxy isomers (3S, 4S, 3G, 4G in Fig. S3).

5-MeO-DALT

Sulfates and glucuronides were found for alkyl hydroxy (13S, 13G in Fig. S4), aryl hydroxy (14S, 14G in Fig. S4), *N*-dealkyl alkyl hydroxy (5S, 5G in Fig. S4), *N*-dealkyl aryl hydroxy (6S, 6G in Fig. S4), *O*-demethyl (7S, 7G in Fig. S4), *O*-demethyl *N*-dealkyl (2S, 2G in Fig. S4), and *O*-demethyl *N*-dealkyl alkyl hydroxy (4S, 4G in Fig. S4) isomers. For *O*-demethyl alkyl hydroxy (9G in Fig. S4) and *O*-demethyl aryl hydroxy (8G in Fig. S4) metabolites, only glucuronides could be observed. Again, in addition to the fragment ions described for phase I metabolites, fragment ions with *m/z* 240.0325 (2S, 7S in Fig. S4), 256.0274 (4S in Fig. S4), 270.0431 (5S, 6S, 13S, 14S in Fig. S4), 336.1078 (2G, 7G in Fig. S4), 352.1027 (4G, 8G, 9G in Fig. S4), or 366.1183 (5G, 6G, 13G, 14G in Fig. S4) were detected for sulfates or glucuronides of metabolites with hydroxy groups on the ethylindole moiety (sections 1+2).

Proposed metabolic pathways

According to the identified metabolites, metabolic pathways could be proposed as depicted in Fig. 2 for DALT and in Fig. 3 for 5-MeO-DALT.

DALT

Three hydroxylations were expected on the indole ring although only two of them could be detected (7, 8 in Fig. 2), most probably due to insufficient separation or low abundance of the third isomer. These mono-hydroxy metabolites were further hydroxylated to two isomeric di-hydroxy metabolites

(9, 10) and these finally to a tri-hydroxy metabolite (13). Aliphatic hydroxylation in section 2 formed a precursor for the corresponding oxo metabolite (5) and the ring-rearranged metabolite (6). *N*-dealkylation (2) and *N*-oxidation could also be observed. The following combinations could be proposed from these observations: aromatic and aliphatic hydroxylation in section 2 (11), *N*-oxidation with aliphatic hydroxylation in section 3 (12), and *N*-dealkylation with aromatic hydroxylation (3, 4). Glucuronidation and sulfation could be observed for both isomers of the aryl hydroxylated metabolites with (3, 4) and without (7, 8) *N*-dealkylation.

5-MeO-DALT

The metabolic pathways were similar to those observed for DALT including aromatic and aliphatic hydroxylation at various sites. Again, the indole ring was expected to bear three different hydroxylation sites but although only one of them could be detected (14 in Fig. 3), presumable due to similar reasons mentioned above. These mono-hydroxy metabolites were further hydroxylated to two isomeric di-hydroxy metabolites (16, 17) and finally to a tri-hydroxy metabolite (20). Aliphatic hydroxylation in section 2 (13) formed a precursor for the corresponding two oxo metabolites (10, 11) and the ring-rearranged metabolite (12). *N*-Dealkylation (3), *N*-oxidation, or *O*-demethylation (7) could also be observed. The following combinations could be proposed: aromatic and aliphatic hydroxylation in section 2 (19), *N*-oxidation with aliphatic mono- or di-hydroxylation in section 3 (18, 21), *N*-dealkylation with aliphatic (5) or aromatic (6) hydroxylation, *O*-demethylation with aliphatic (9) or aromatic mono- (8) or di-hydroxylation (15), with *N*-dealkylation (2), or *N*-dealkylation with aliphatic hydroxylation (4). Glucuronidation and sulfation could be observed for alkyl (13) or aryl hydroxy metabolites (14), for *O*-demethyl (7) or *N*-dealkyl metabolites (3), and *O*-demethyl hydroxy metabolites (2, 4-6). For *O*-demethyl alkyl (9) or aryl hydroxy metabolites (8), only glucuronides were detected.

Comparing the pathways of both drugs, it is obvious that one of the di-hydroxy metabolites of DALT (9 in Fig. 2) should be identical to the *O*-demethyl hydroxy metabolite of 5-MeO-DALT (8 in Fig. 3). Similarly, the tri-hydroxy metabolite of DALT (13 in Fig. 2) would be identical to the *O*-demethyl di-hydroxy metabolite of 5-MeO-DALT (15 in Fig. 3), thus, accounting for identical spectra and retention times. The *O*-demethyl metabolite of 5-MeO-DALT (7 in Fig. 3) could be identical either to the hydroxy metabolite 7 (Fig. 2) of DALT with slightly different spectra and retention times or to the undetected hydroxy metabolite.

Microsomal incubations of DALT and 5-MeO-DALT

Unfortunately, no human urine samples were available to confirm that the metabolites in rat urine would also be found in human urine. According to many former studies [16, 20, 27-34], combination of rat urine studies with incubations of new drugs with pHLM provides a tool for good predictions of phase I metabolites for detection in human urine. Katagi et al. discussed the transferability for other *N,N*-di-alkyl tryptamines [16]. After pHLM incubation, all phase I metabolites could be detected for DALT and metabolites 3, 5-7, 10-14, 16-18, and 21 (Fig. 3) for 5-MeO-DALT. Therefore, it seems reasonable to assume that at least some of these metabolites might also be found in human urine.

For the initial CYP activity screening, the metabolites were detected after incubation with individual CYPs. The relative involvement of the single CYPs in metabolic pathways of DALT are given in Table 1 and those of 5-MeO-DALT in Table 2. The relative involvement of individual CYPs was defined in relation to the highest peak abundances during precursor ion monitoring of the formed metabolites. A CYP was defined as mainly involved if the corresponding relative peak abundance values were above 50 %. According to these findings, the following isoenzymes were mainly involved in given metabolic steps: for DALT, CYP3A4 in all types of hydroxylations, CYP2D6 in oxidation to the oxo metabolite, CYP2C19 and CYP3A4 in *N*-dealkylations; for 5-MeO-DALT, CYP3A4 in all type of hydroxylations, CYP1A2 and CYP2D6 in oxidation to the oxo metabolites,

CYP2C19 and CYP3A4 in *N*-dealkylations, and CYP2D6 in *O*-demethylations. Given that several CYP enzymes were involved in the metabolism of both drugs, one might expect that CYP enzyme polymorphisms might be of minor toxicological relevance.

Toxicological detection of DALT and 5-MeO-DALT by GC-MS, LC-MS^n, and LC-HR-MS/MS

The doses of 1 mg/kg BM administered to rats corresponded to low human single doses of about 10 mg scaled by dose-by-factor approach according to Sharma et al. [35]. As described above, these doses corresponded to the suggested dose for 5-MeO-DALT [9-11]. The corresponding urine samples were used for the detectability studies. As already discussed, no human urine samples were available and thus, the main target for human urinalysis could not be elucidated. However, the SUSAs cover all metabolites detected in rat urine including those identified in pHLM with their conjugates. From the experience gained in the last years, the possibility that consumption of these drugs and identification of their metabolites could be overlooked seems rather low.

Using GC-MS, only DALT could be screened for via the metabolites given in Table 3 with the corresponding fragment ions, their relative abundances, and their retention indices. 5-MeO-DALT and its metabolites could be monitored only in rat urine after high dose administration and might therefore be detectable only in overdose cases. The corresponding GC-MS data are published elsewhere [23].

Using LC-MS^n, both drugs could be screened for via the metabolites given in Table 4 using the protonated precursor ions, characteristic MS^2 and MS^3 fragment ions, and retention times. The LC-HR-MS/MS SUSA allowed for monitoring an intake of both drugs by detecting the following metabolites with the given HR-MS/MS spectra: for DALT, spectra nos. 1, 4, 7, 10, 13 in Fig. S1 and 3S, 4S, 8S, 3G, 4G, 7G, 8G in Fig. S3; for 5-MeO-DALT, spectra nos. 2 in Fig. S2 and 7S, 13S, 5G, 6G, 7G, 9G, 13G, 14G in Fig. S4. Reconstructed LC-HR-MS/MS ion chromatograms with the given *m/z* of the most abundant metabolites following work-up of a rat urine sample (low dose) are depicted

in Fig. 4. The metabolites of DALT (part A) with the most abundant peak areas were aryl-hydroxy-glucuronide isomer 1 (7G in Fig. S3), its isomer 2 (8G in Fig. S3), aryl-hydroxy isomer 1 (7 in Fig. S1), and aryl-tri-hydroxy metabolite (13 in Fig. S1). The metabolites of 5-MeO-DALT (part B) with the most abundant peak areas were *O*-demethyl-glucuronide (7G in Fig. S4), alkyl-hydroxy-glucuronide (13G in Fig. S4), *N*-dealkyl-aryl-hydroxy-glucuronide (6G in Fig. S4), aryl-hydroxy-glucuronide (14G in Fig. S4), and *N*-dealkyl-alkyl-hydroxy-glucuronide metabolite (5G in Fig. S4), respectively. Fortunately, because various targets could be detected, the risk of false negative results caused by ion suppression of a particular target was limited.

To assess the general performance of the SUSAs, the limits of detection (LOD) for the parent compounds were determined in the particular approaches although they were not the main targets chosen for urinalysis. Urine samples spiked with the corresponding drugs in decreasing concentrations were analyzed with all SUSAs and the signal-to-noise ratio of 3 was defined as LOD. For GC-MS, LC-MS^n, and LC-HR-MS/MS SUSA, the LODs for DALT in urine were 10, 10, and 1 ng/mL and for 5-MeO-DALT 50, 10, and 1 ng/mL, respectively. Considering the fact, that for GC-MS, 5 mL and for both LC-MS approaches only 0.1 mL of urine was processed for work-up, the LODs for DALT were comparable for GC-MS and LC-MS^n, but as expected much lower for LC-HR-MS/MS. The rather high LOD for 5-MeO-DALT in GC-MS might be caused by reduced ionization, as the peak area of the reference standards also differed in the same range.

Conclusions

The two new psychoactive substances DALT and 5-MeO-DALT were extensively metabolized in rats. It could be assumed that those metabolites should also be found in human urine considering the results obtained from pHLM incubations. CYP2C19, CYP2D6, and CYP3A4 were mainly involved in DALT and 5-MeO-DALT metabolism. The LC-MS^n and LC-HR-MS/MS SUSAs should be

suitable for reliably monitoring an intake of both drugs. The GC-MS SUSA should be able to monitor DALT intake, but 5-MeO-DALT only in overdose cases.

Acknowledgements The authors like to thank Achim T. Caspar, Julia Dinger, Golo M. J. Meyer, Jessica Welter, Carina S. D. Wink, Carsten Schröder, Gabriele Ulrich, and Armin A. Weber for their support and/or helpful discussion.

References

1. United Nations Office on Drugs and Crime (UNODC) (2014) World Drug Report 2014. http://www.unodc.org/documents/data-and-analysis/WDR2014/World_Drug_Report_2014_web.pdf
2. Brandt SD, King LA, Evans-Brown M (2014) The new drug phenomenon. Drug Test Anal 6:587-597
3. Meyer MR, Caspar A, Brandt SD, Maurer HH (2014) A qualitative/quantitative approach for the detection of 37 tryptamine-derived designer drugs, 5 beta-carbolines, ibogaine, and yohimbine in human urine and plasma using standard urine screening and multi-analyte approaches. Anal Bioanal Chem 406:225-237
4. Blough BE, Landavazo A, Decker AM, Partilla JS, Baumann MH, Rothman RB (2014) Interaction of psychoactive tryptamines with biogenic amine transporters and serotonin receptor subtypes. Psychopharmacology (Berl) 231:4135-4144
5. Cozzi NV, Gopalakrishnan A, Anderson LL, Feih JT, Shulgin AT, Daley PF, Ruoho AE (2009) Dimethyltryptamine and other hallucinogenic tryptamines exhibit substrate behavior at the serotonin uptake transporter and the vesicle monoamine transporter. J Neural Transm 116:1591-1599
6. Halberstadt AL, Geyer MA (2011) Multiple receptors contribute to the behavioral effects of indoleamine hallucinogens. Neuropharmacology 61:364-381
7. Halberstadt AL, Koedood L, Powell SB, Geyer MA (2011) Differential contributions of serotonin receptors to the behavioral effects of indoleamine hallucinogens in mice. J Psychopharmacol 25:1548-1561
8. Nichols DE (2012) Structure-activity relationships of serotonin 5-HT_{2A} agonists. WIREs Membr Transp Signal 1:559-579

9. Shulgin AT (2003) Basic Pharmacology and Effects. In: Laing, R. R. Halluinogens. A Forensic Drug Handbook. Elsevier Science, London 67-137

10. Shulgin AT, Shulgin A (2004) 5-MeO-DALT. http://isomerdesign.com/PiHKAL/read.php?domain=tk&id=56

11. Shulgin AT, Shulgin A (2004) DALT. http://isomerdesign.com/PiHKAL/read.php?domain=tk&id=57

12. Corkery JM, Durkin E, Elliott S, Schifano F, Ghodse AH (2012) The recreational tryptamine 5-MeO-DALT (N,N-diallyl-5-methoxytryptamine): a brief review. Prog Neuropsychopharmacol Biol Psychiatry 39:259-262

13. Jovel A, Felthous A, Bhattacharyya A (2014) Delirium due to intoxication from the novel synthetic tryptamine 5-MeO-DALT. J Forensic Sci 59:844-846

14. Brandt SD, Martins CPB (2010) Analytical methods for psychoactive *N*,*N*-dialkylated tryptamines. Trends Anal Chem 29:858-869

15. Gaujac A, Navickiene S, Collins MI, Brandt SD, de Andrade JB (2012) Analytical techniques for the determination of tryptamines and beta-carbolines in plant matrices and in psychoactive beverages consumed during religious ceremonies and neo-shamanic urban practices. Drug Test Anal 4:636-648

16. Katagi M, Kamata T, Zaitsu K, Shima N, Kamata H, Nakanishi K, Nishioka H, Miki A, Tsuchihashi H (2010) Metabolism and toxicologic analysis of tryptamine-derived drugs of abuse. Ther Drug Monit 32:328-331

17. Brandt SD, Tirunarayanapuram SS, Freeman S, Dempster N, Barker SA, Daley PF, Cozzi NV, Martins CPB (2008) Microwave-accelerated synthesis of psychoactive deuterated N,N-dialkylated-[alpha,alpha,beta,beta-d(4)]-tryptamines. J Label Compd Radiopharm 51:423-429

18. Wissenbach DK, Meyer MR, Remane D, Weber AA, Maurer HH (2011) Development of the first metabolite-based LC-MSn urine drug screening procedure - exemplified for antidepressants. Anal Bioanal Chem 400:79-88

19. Meyer MR, Vollmar C, Schwaninger AE, Maurer HH (2012) New cathinone-derived designer drugs 3-bromomethcathinone and 3-fluoromethcathinone: studies on their metabolism in rat urine and human liver microsomes using GC-MS and LC-high-resolution MS and their detectability in urine. J Mass Spectrom 47:253-262

20. Helfer AG, Turcant A, Boels D, Ferec S, Lelievre B, Welter J, Meyer MR, Maurer HH (2015) Elucidation of the metabolites of the novel psychoactive substance 4-methyl-*N*-ethyl-cathinone (4-MEC) in human urine and pooled liver microsomes by GC-MS and LC-HR-MS/MS techniques and of its detectability by GC-MS or LC-MS^n standard screening approaches. Drug Test Anal 7:368-375

21. Maurer HH, Pfleger K, Weber AA (2011) Mass Spectral and GC Data of Drugs, Poisons, Pesticides, Pollutants and their Metabolites. Wiley-VCH, Weinheim (Germany)

22. Welter J, Kavanagh P, Maurer HH (2014) GC-MS and LC-(high-resolution)-MS^n studies on the metabolic fate and detectability of camfetamine in rat urine. Anal Bioanal Chem 406:3815-3829

23. Maurer HH, Pfleger K, Weber AA (2015) Mass Spectral Library of Drugs, Poisons, Pesticides, Pollutants and their Metabolites. Wiley-VCH, Weinheim

24. Meyer MR, Peters FT, Maurer HH (2010) Automated mass spectral deconvolution and identification system for GC-MS screening for drugs, poisons, and metabolites in urine. Clin Chem 56:575-584

25. Maurer HH, Wissenbach DK, Weber AA (2014) Maurer/Wissenbach/Weber MWW LC-MSn Library of Drugs, Poisons, and their Metabolites. Wiley-VCH, Weinheim (Germany)

26. Niessen WMA (2011) Fragmentation of Toxicologically Relevant Drugs in Positive-Ion Liquid Chromatography-Tandem Mass Spectrometry. Mass Spectrometry Reviews 30:626-663

27. Caspar AT, Helfer AG, Michely JA, Auwaerter V, Brandt SD, Meyer MR, Maurer HH (2015) Studies on the metabolism and toxicological detection of the new psychoactive designer drug 2-(4-iodo-2,5-dimethoxyphenyl)-N-[(2-methoxyphenyl)methyl]ethanamine (25I-NBOMe) in human and rat urine using GC-MS, LC-MSn, and LC-HR-MS/MS. Anal Bioanal Chem DOI: 10.1007/s00216-015-8828-6

28. Welter J, Kavanagh P, Meyer MR, Maurer HH (2015) Benzofuran analogues of amphetamine and methamphetamine: studies on the metabolism and toxicological analysis of 5-APB and 5-MAPB in urine and plasma using GC-MS and LC-(HR)-MS^n techniques. Anal Bioanal Chem 407:1371-1388

29. Wink CSD, Meyer MR, Braun T, Turcant A, Maurer HH (2015) Biotransformation and detectability of the designer drug 2,5-dimethoxy-4-propylphenethylamine (2C-P) studied in urine by GC-MS, LC-MS^n and LC-high resolution-MS^n. Anal Bioanal Chem 407:831-843

30. Meyer MR, Mauer S, Meyer GMJ, Dinger J, Klein B, Westphal F, Maurer HH (2014) The in vivo and in vitro metabolism and the detectability in urine of 3',4'-methylenedioxy-alpha-pyrrolidinobutyrophenone (MDPBP), a new pyrrolidinophenone-type designer drug, studied by GC-MS and LC-MSn. Drug Test Anal 6:746-756

31. Welter J, Meyer MR, Wolf E, Weinmann W, Kavanagh P, Maurer HH (2013) 2-Methiopropamine, a thiophene analogue of methamphetamine: studies on its metabolism and detectability in the rat and human using GC-MS and LC-(HR)-MS techniques. Anal Bioanal Chem 405:3125-3135

32. Meyer MR, Wilhelm J, Peters FT, Maurer HH (2010) Beta-keto amphetamines: studies on the metabolism of the designer drug mephedrone and toxicological detection of mephedrone,

butylone, and methylone in urine using gas chromatography-mass spectrometry. Anal Bioanal Chem 397:1225-1233

33. Philipp AA, Wissenbach DK, Weber AA, Zapp J, Zoerntlein SW, Klein ON, Kanogsunthornrat J, Maurer HH (2010) Use of liquid chromatography coupled to low- and high-resolution linear ion trap mass spectrometry for studying the metabolism of paynantheine, an alkaloid of the herbal drug Kratom in rat and human urine. Anal Bioanal Chem 396:2379-2391
34. Philipp AA, Wissenbach DK, Weber AA, Zapp J, Maurer HH (2010) Phase I and II metabolites of speciogynine, a diastereomer of the main *Kratom* alkaloid mitragynine, identified in rat and human urine by liquid chromatography coupled to low and high resolution linear ion trap mass spectrometry. J Mass Spectrom 45:1344-1357
35. Sharma V, McNeill JH (2009) To scale or not to scale: the principles of dose extrapolation. Br J Pharmacol 157:907-921
36. Kovats E (1958) Gaschromatographische Charakterisierung organischer Verbindungen. Teil 1. Retentionsindices aliphatischer Halogenide, Alkohole, Aldehyde und Ketone. Helv Chim Acta 41:1915-1932

Table 1 Relative involvement of human CYP isoenzymes in metabolic pathways of DALT

CYP isoenzymes	Hydroxylations, all types (%)	Oxidations to oxo metabolites (%)	*N*-dealkylations (%)
CYP1A2	11	35	46
CYP2A6	1	0	1
CYP2B6	12	4	5
CYP2C8	3	0	5
CYP2C9	3	2	20
CYP2C19	4	13	69
CYP2D6	25	100	25
CYP2E1	3	0	5
CYP3A4	100	5	100
CYP3A5	0	0	0

Table 2 Relative involvement of human CYP isoenzymes in metabolic pathways of 5-MeO-DALT

CYP isoenzymes	Hydroxylations, all types (%)	Oxidations to oxo metabolites (%)	*N*-dealkylations (%)	*O*-Demethylations (%)
CYP1A2	1	100	23	0
CYP2A6	0	0	1	0
CYP2B6	0	3	3	0
CYP2C8	0	0	5	0
CYP2C9	1	0	39	3
CYP2C19	0	20	100	21
CYP2D6	0	92	29	100
CYP2E1	0	0	1	0
CYP3A4	100	17	88	15
CYP3A5	0	0	5	0

Table 3 Targets for GC-MS SUSA monitoring DALT with molecular masses, five most abundant fragment ions, their relative abundances, and retention indices according to Kovats [36]

Compound	**Molecular mass (u)**	**GC-MS fragment ions (*m/z*) and their relative abundance (%)**	**Retention index**
DALT-M (HO-) AC	298	110 (100), 146 (9), 160 (3), 257 (1), 298 (1)	2310
DALT-M (*N*-dealkyl-HO-) 2AC	300	159 (100), 70 (59), 146 (56), 201 (53), 300 (10)	2690
DALT-M (tri-HO-) 3AC	414	110 (100), 373 (15), 146 (10), 160 (3), 414 (1)	2400

Table 4 Targets for LC-MS^n SUSA monitoring DALT or 5-MeO-DALT with protonated precursor ions, characteristic MS^2 and MS^3 fragment ions, and retention time (RT)

Targets for SUSA	**Precursor ions (*m/z*)**	**MS^2 fragment ions (*m/z*), and relative intensity (%)**	**MS^3 fragment ions (*m/z*) on the ion given in bold and relative intensity (%)**	**RT (min)**
DALT-M (*N*-dealkyl-HO-aryl-glucuronide)	393	160 (100), 217 (87), 148 (47), 336 (38), 324 (21)	**160**: 132 (100), 160 (79), 116 (64)	1.5
DALT-M (tri-HO-aryl-)	289	110 (100), 247 (7), 192 (5), 176 (4), 229 (3)	**110**: 81 (100), 69 (12), 79 (11), 68 (10), 69 (10)	2.3
DALT-M (HO-aryl-glucuronide) isomer 1	433	257 (100), 336 (39), 160 (33), 215 (1), 376 (1)	**257**: 110 (100), 160 (62), 111 (7), 98 (3), 77 (2)	2.9
DALT-M (HO-aryl-glucuronide) isomer 2	433	336 (100), 160 (36), 257 (20), 318 (2), 405 (1)	**336**: 160 (100), 132 (2), 115 (1)	4.7
DALT-M (di-HO-aryl-)	273	176 (100), 231 (91), 232 (68), 148 (21), 174 (8)	**176**: 148 (100), 130 (3), 82 (1)	5.2
DALT-M (HO-aryl-)	257	110 (100), 160 (6), 215 (3), 79 (1), 82 (1)	**110**: 81 (100), 68 (29), 80 (19), 70 (11), 55 (9)	5.3
5-MeO-DALT-M (*N*-dealkyl-HO-alkyl-glucuronide)	423	178 (100), 366 (65), 354 (38), 190 (29), 247 (29)	**178**: 146 (100), 118 (9), 122 (3)	1.6
5-MeO-DALT-M (*O*-demethyl-glucuronide)	433	257 (100), 160 (33), 336 (23)	**257**: 110 (100), 160 (76), 98 (2), 81 (1), 80 (1)	3.0
5-MeO-DALT-M (HO-aryl-glucuronide)	273	366 (100), 287 (74), 190 (41), 164 (3), 348 (3)	**366**: 190 (100), 158 (2), 175 (2)	5.0

Legends to Figures

Fig. 1 Structure of DALT (A) and 5-MeO-DALT (B) with corresponding division into sections to aid the identification procedure of metabolites

Fig. 2 Proposed metabolic pathways for DALT (numbering according to Fig. S1)

Fig. 3 Proposed metabolic pathways for 5-MeO-DALT (numbering according to Fig. S2)

Fig. 4 Reconstructed LC-HR-MS ion chromatograms with the corresponding protonated molecular exact masses (+/- 5 ppm) indicating the given DALT metabolites (part A) and 5-MeO-DALT metabolites (part B) in rat urine samples after low dose administration

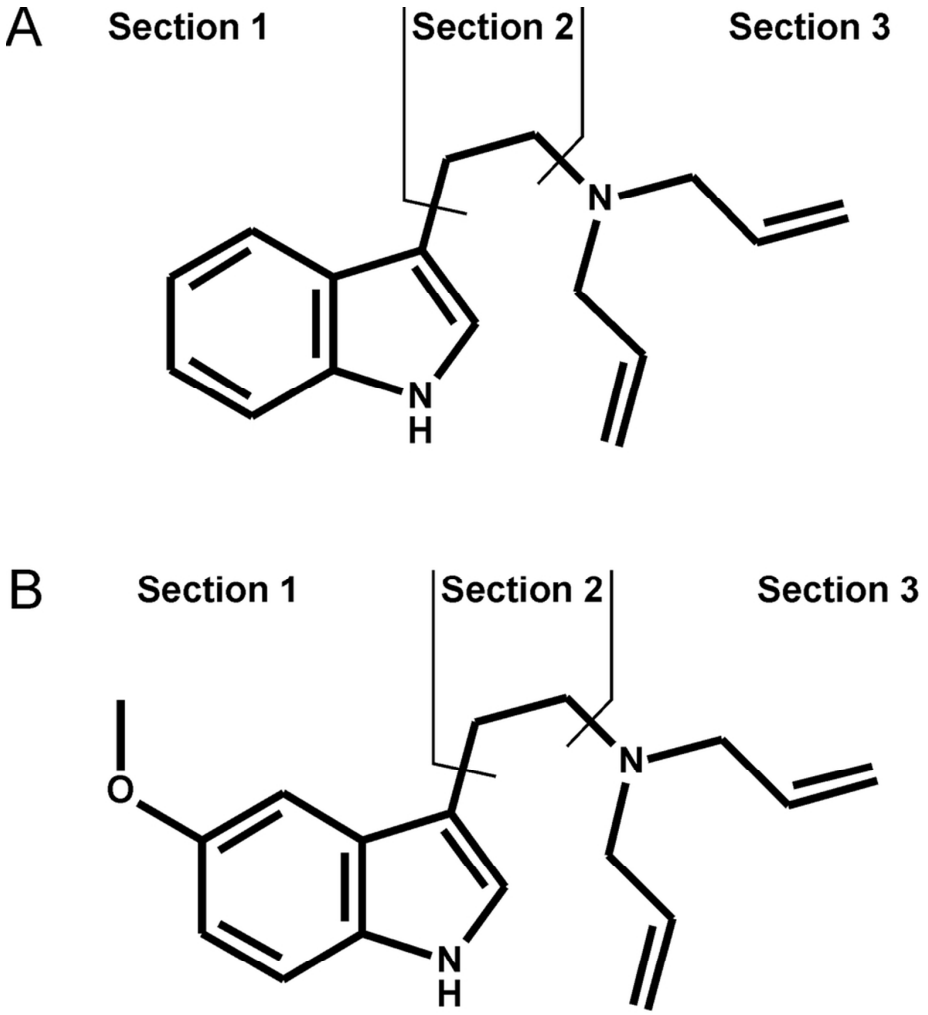

Fig. 1 Structure of DALT (A) and 5-MeO-DALT (B) with corresponding division into sections to aid the identification procedure of metabolites
80x92mm (300 x 300 DPI)

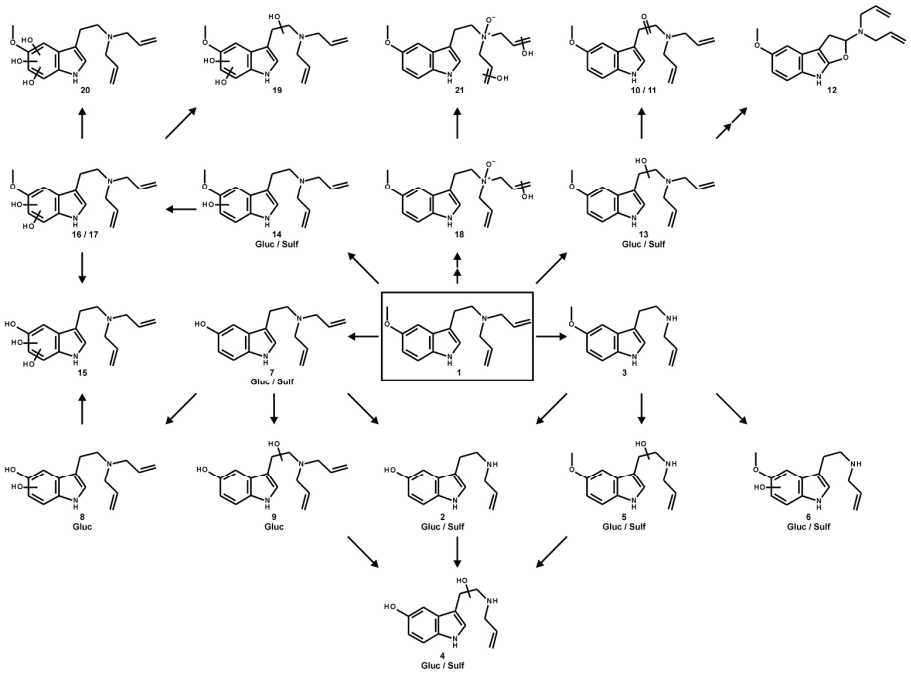

Fig. 3 Proposed metabolic pathways for 5-MeO-DALT (numbering according to Fig. S2)
217x159mm (300 x 300 DPI)

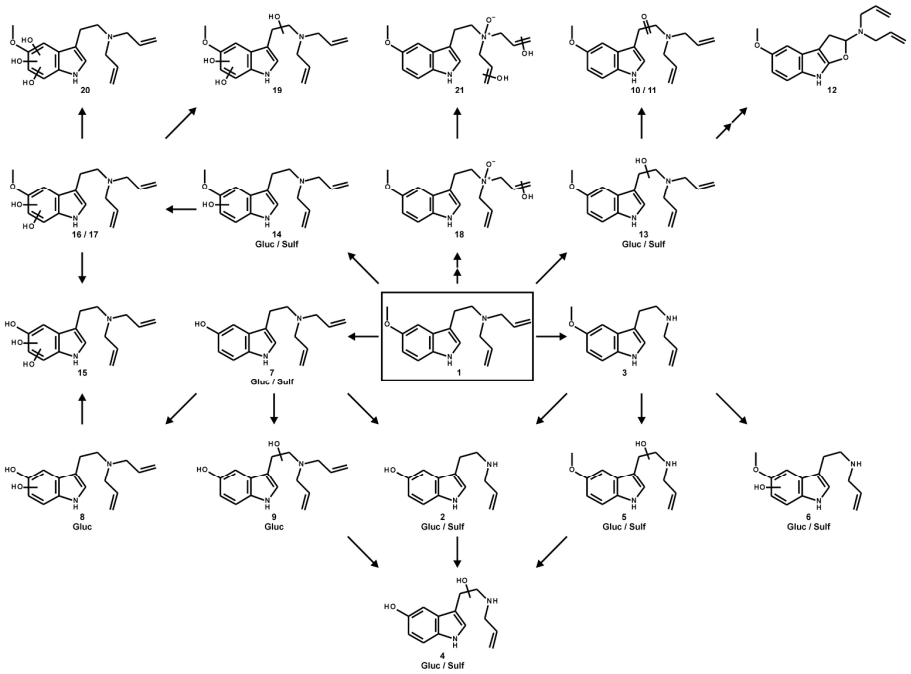

Fig. 3 Proposed metabolic pathways for 5-MeO-DALT (numbering according to Fig. S2)
217x159mm (300 x 300 DPI)

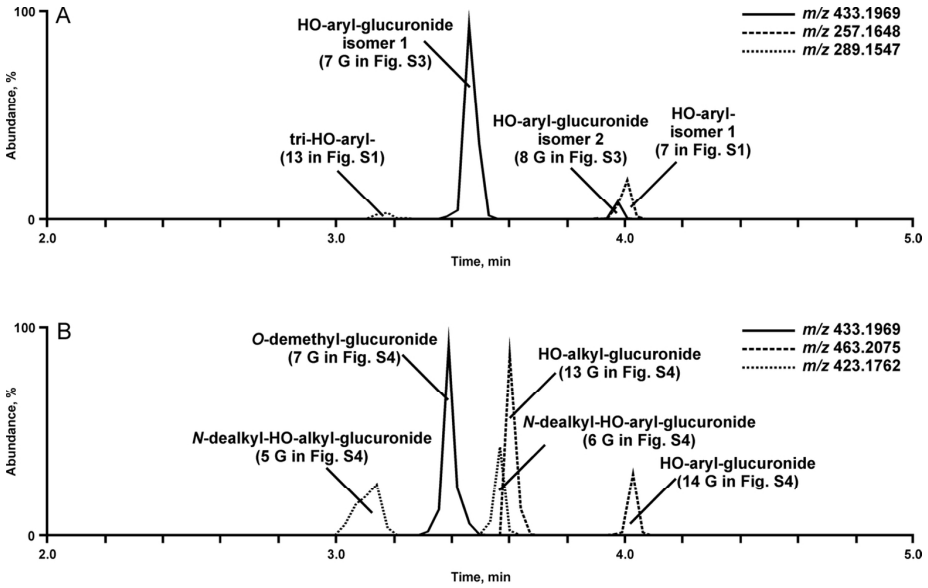

Fig. 4 Reconstructed LC-HR-MS ion chromatograms with the corresponding protonated molecular exact masses (+/- 5 ppm) indicating the given DALT metabolites (part A) and 5-MeO-DALT metabolites (part B) in rat urine samples after low dose administration
125x79mm (300 x 300 DPI)

Analytical and Bioanalytical Chemistry

Electronic Supplementary Material

Metabolism of the new psychoactive substances *N*,*N*-diallyltryptamine (DALT) and 5-methoxy-DALT and their detectability in urine by GC-MS, LC-MS^n, and LC-HR-MS/MS

Julian A. Michely * Andreas G. Helfer * Markus R. Meyer * Hans H. Maurer (corresponding author)

Department of Experimental and Clinical Toxicology, Institute of Experimental and Clinical Pharmacology and Toxicology, Saarland University, 66421 Homburg (Saar), Germany

e-mail: hans.maurer@uks.eu

Simon D. Brandt

School of Pharmacy and Biomolecular Sciences, Liverpool John Moores University, L3 3AF, Liverpool, United Kingdom

Markus R. Meyer

Present address: Farmakologiska laboratoriet, Klinisk farmakologi, Karolinska Universitetssjukhuset Huddinge, Karolinska Institutet, 141 86 Stockholm, Sweden

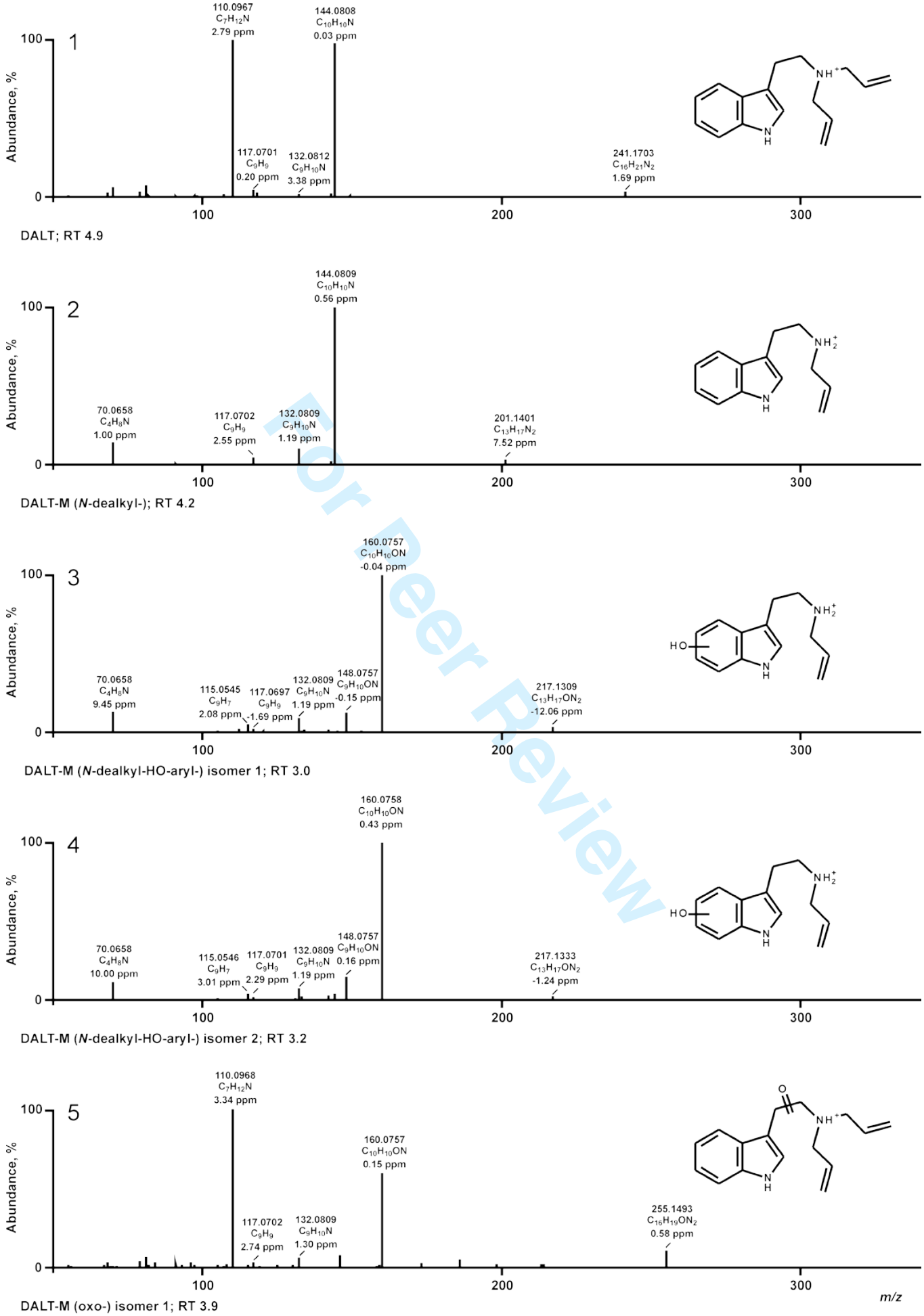

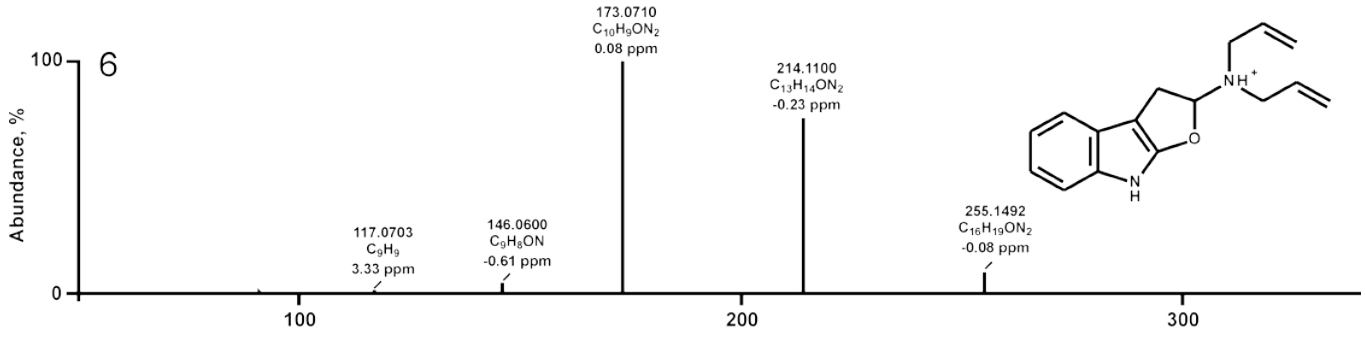

DALT-M (oxo-) isomer 2; RT 4.7

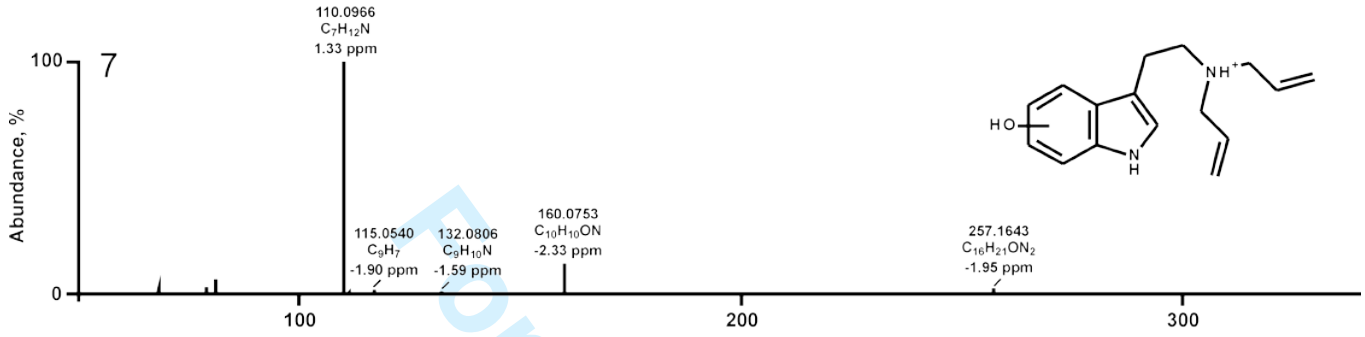

DALT-M (HO-aryl-) isomer 1; RT 3.9

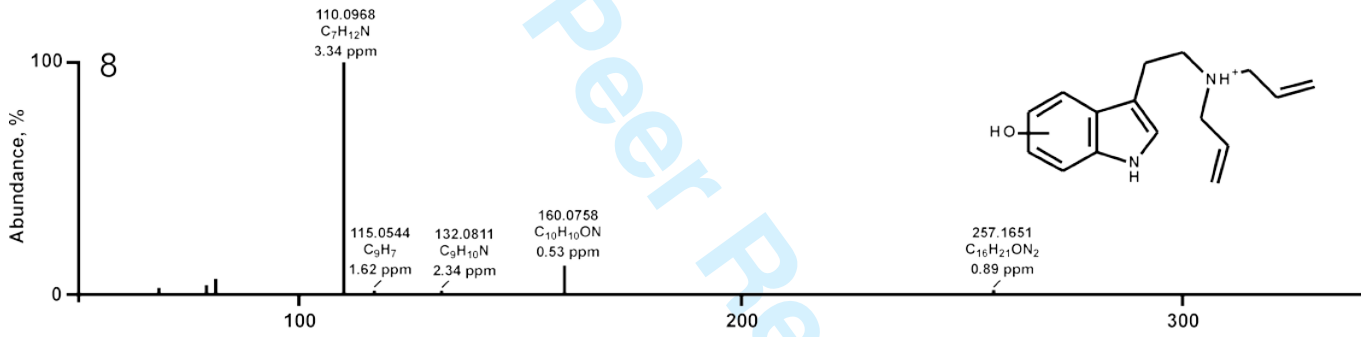

DALT-M (HO-aryl-) isomer 2; RT 4.3

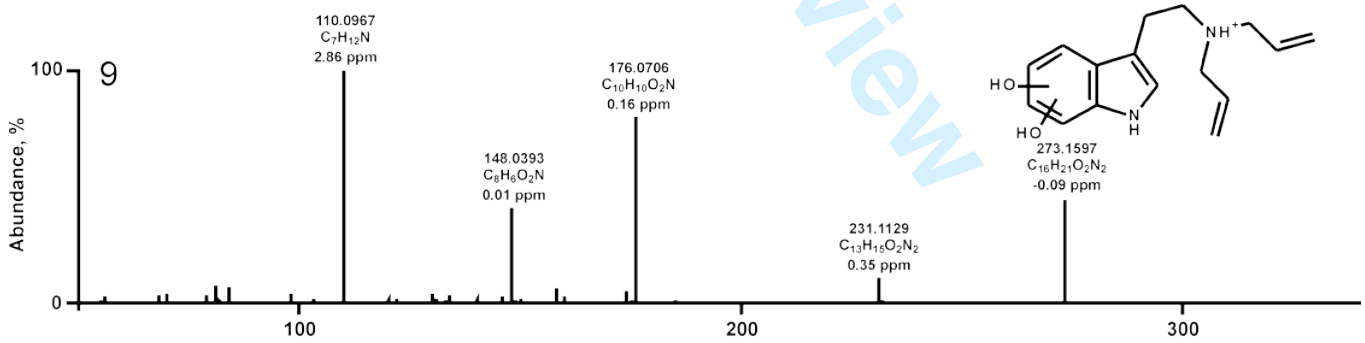

DALT-M (di-HO-aryl-) isomer 1; RT 3.4

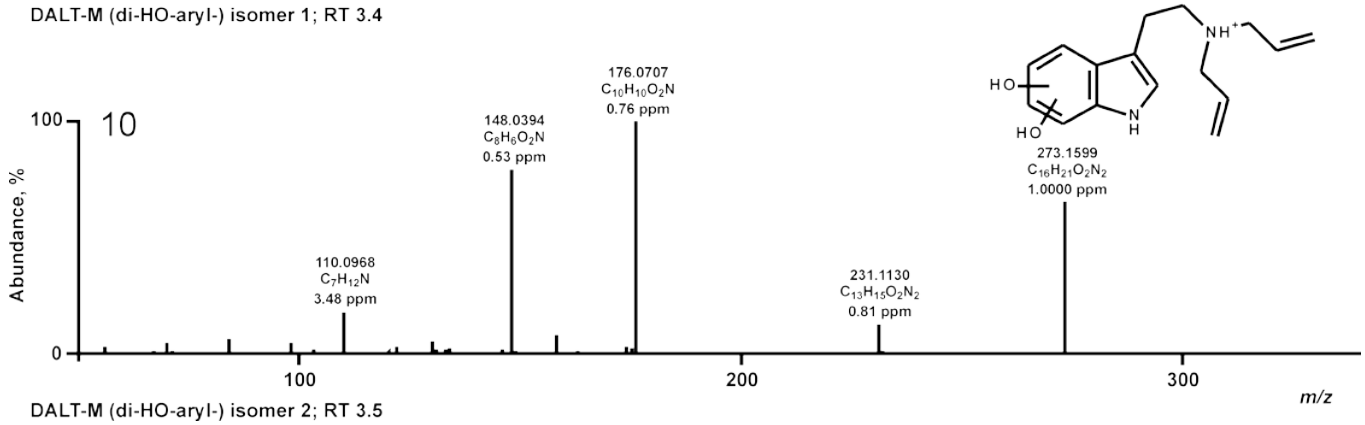

DALT-M (di-HO-aryl-) isomer 2; RT 3.5

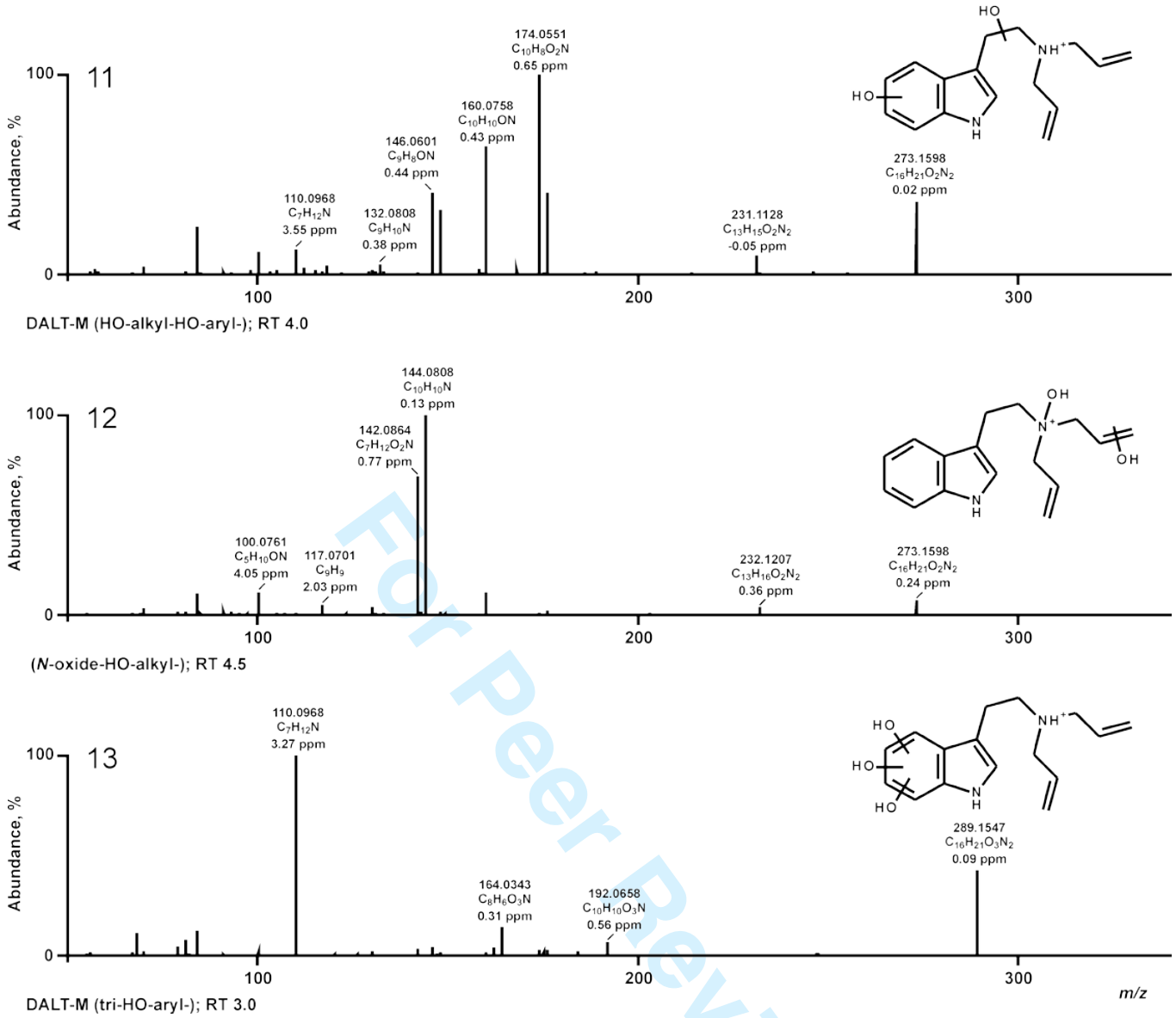

Fig. S1 LC-HR-MS/MS spectra of DALT and its phase I metabolites arranged according to their precursor values, proposed chemical structures, accurate masses, calculated elemental formulas, and mass error values in parts per million (ppm) rounded to two decimals

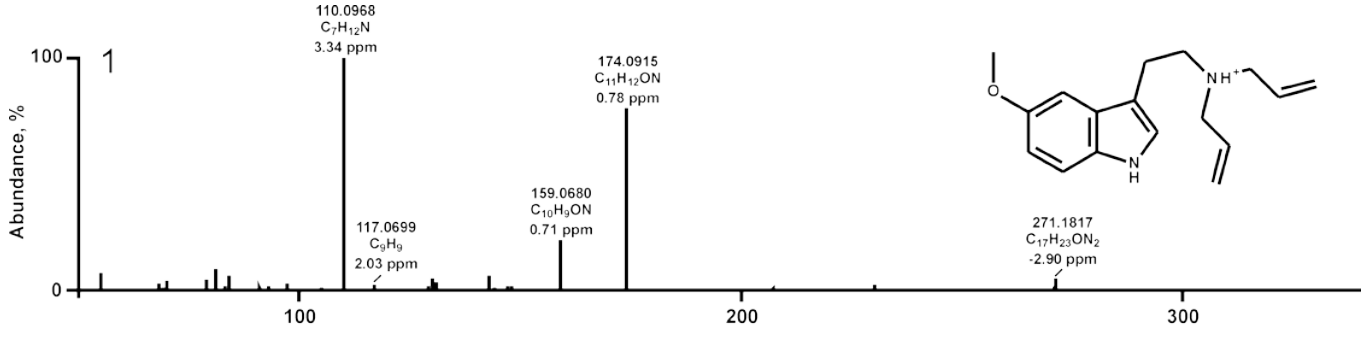

5-MeO-DALT; RT 4.8

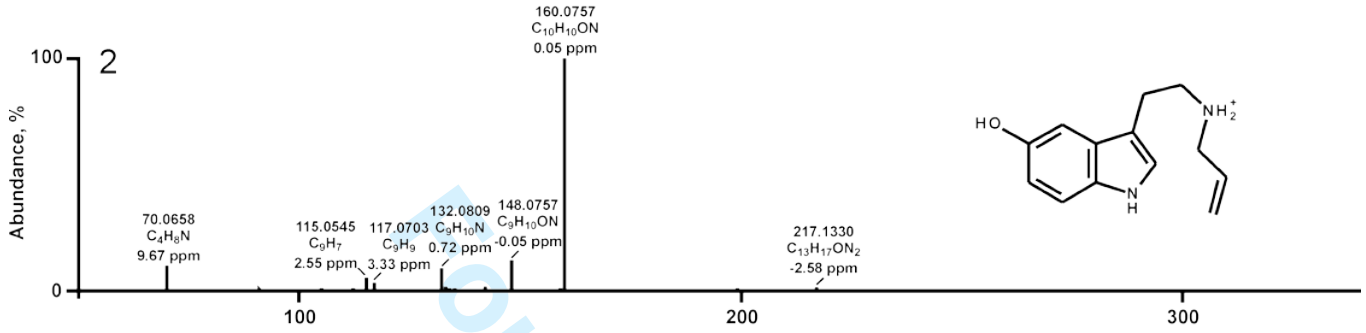

5-MeO-DALT-M (*O*-demethyl-*N*-dealkyl-); RT 3.1

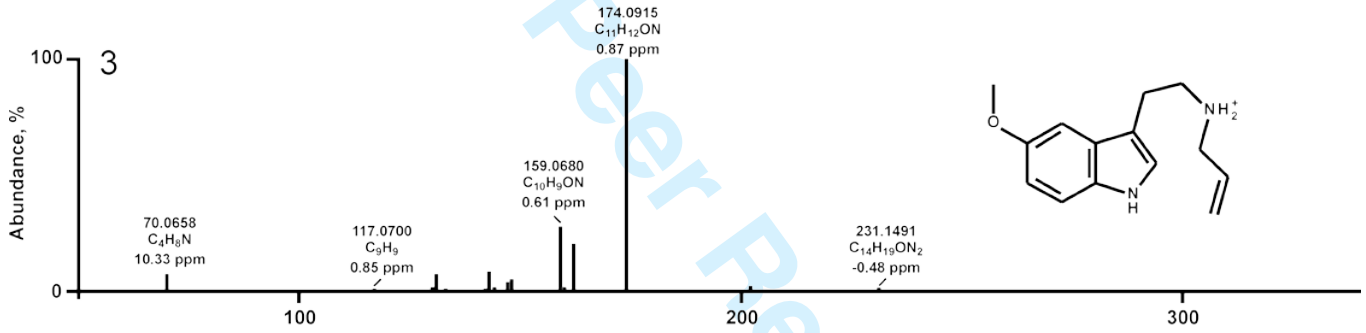

5-MeO-DALT-M (*N*-dealkyl-); RT 4.2

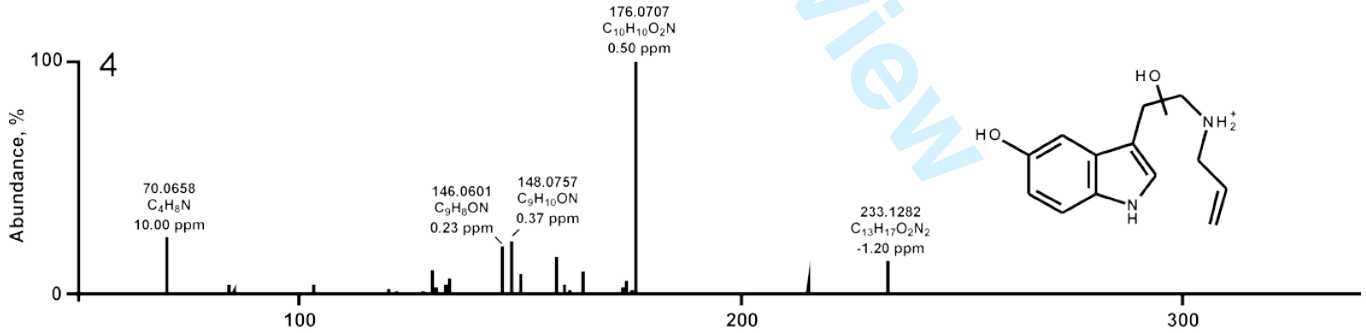

5-MeO-DALT-M (*O*-demethyl-*N*-dealkyl-HO-alkyl-); RT 2.7

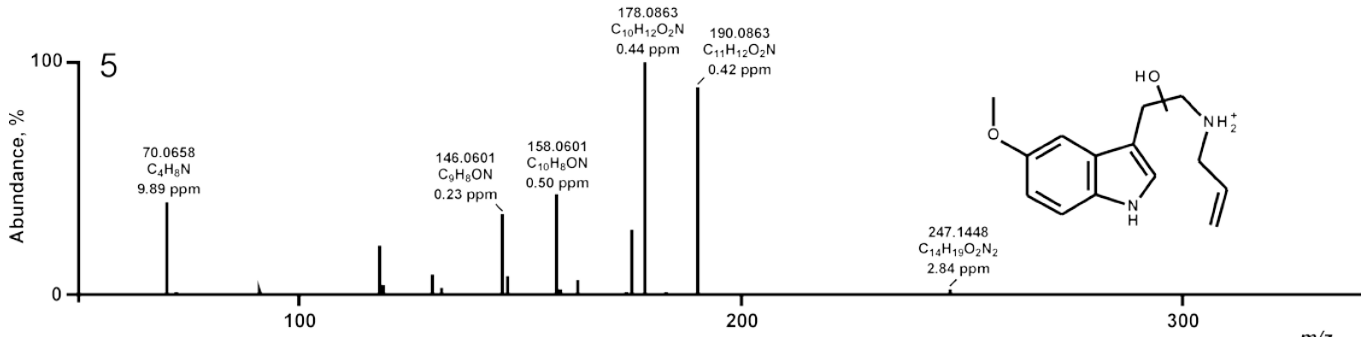

5-MeO-DALT-M (*N*-dealkyl-HO-alkyl-); RT 3.4

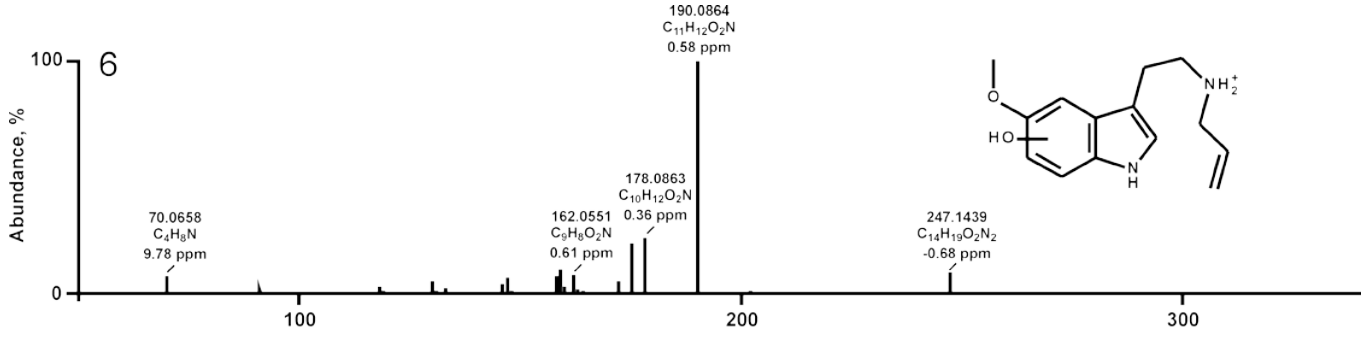

5-MeO-DALT-M (*N*-dealkyl-HO-aryl-); RT 3.7

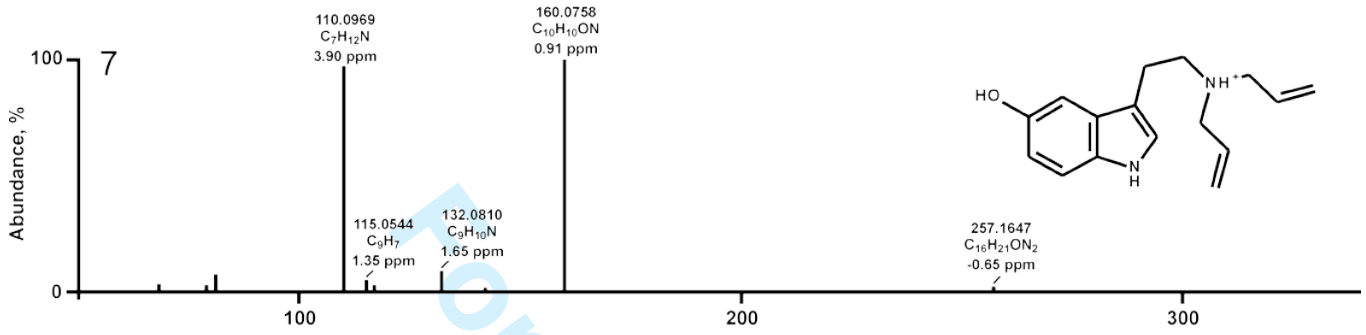

5-MeO-DALT-M (*O*-demethyl-); RT 3.8

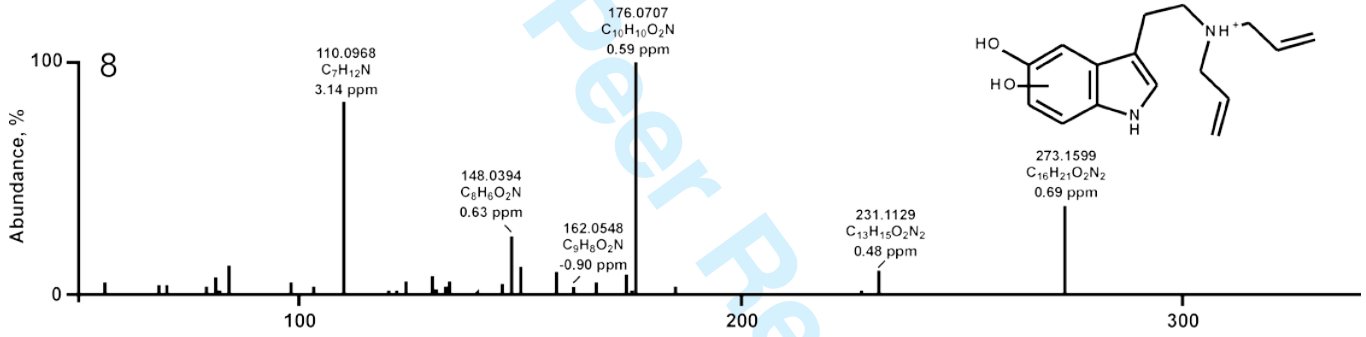

5-MeO-DALT-M (*O*-demethyl-HO-aryl-); RT 3.4

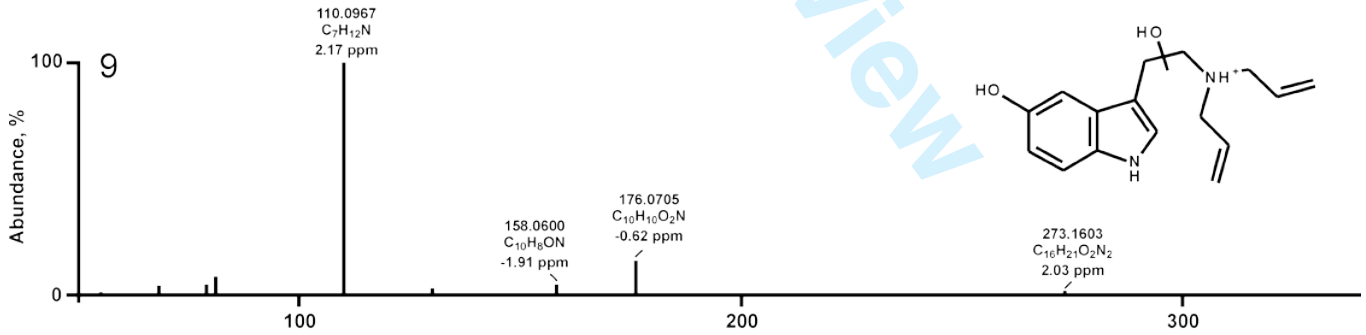

5-MeO-DALT-M (*O*-demethyl-HO-alkyl-); RT 3.5

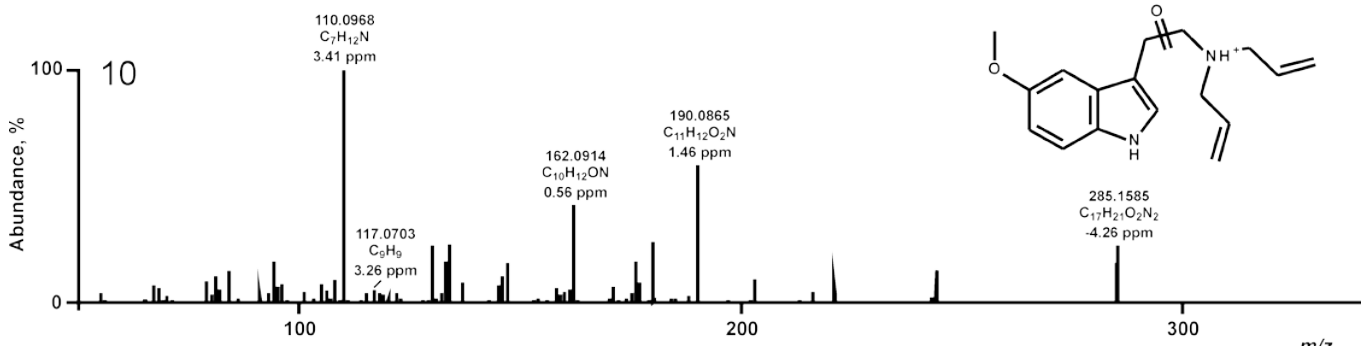

5-MeO-DALT-M (oxo-) isomer 1; RT 3.7

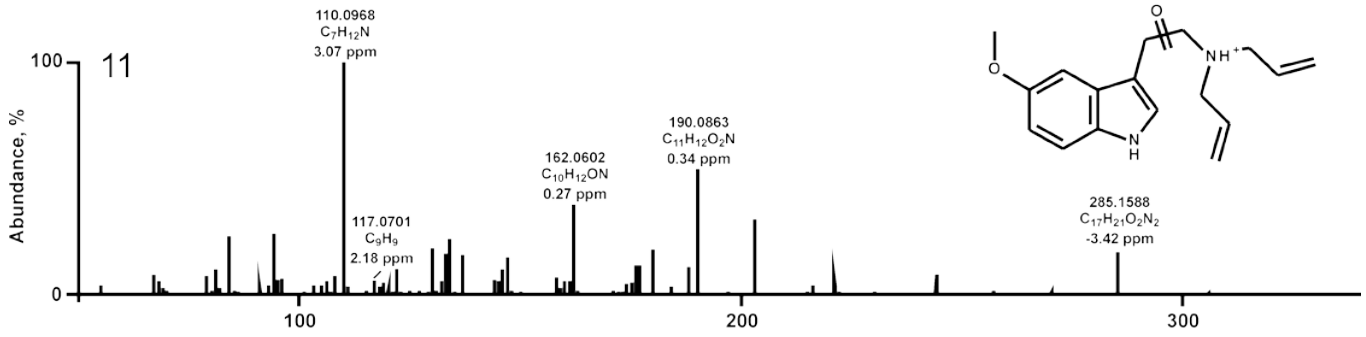

5-MeO-DALT-M (oxo-) isomer 2; RT 4.2

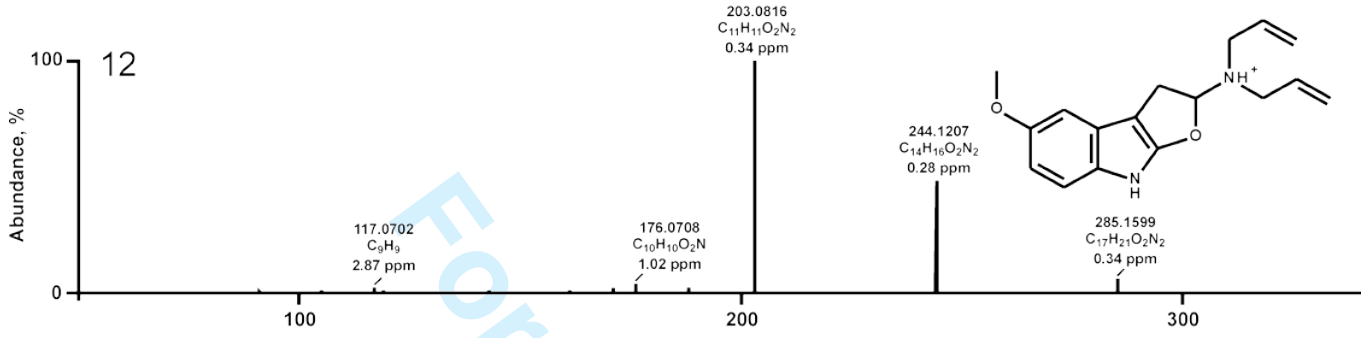

5-MeO-DALT-M (oxo-) isomer 3; RT 4.7

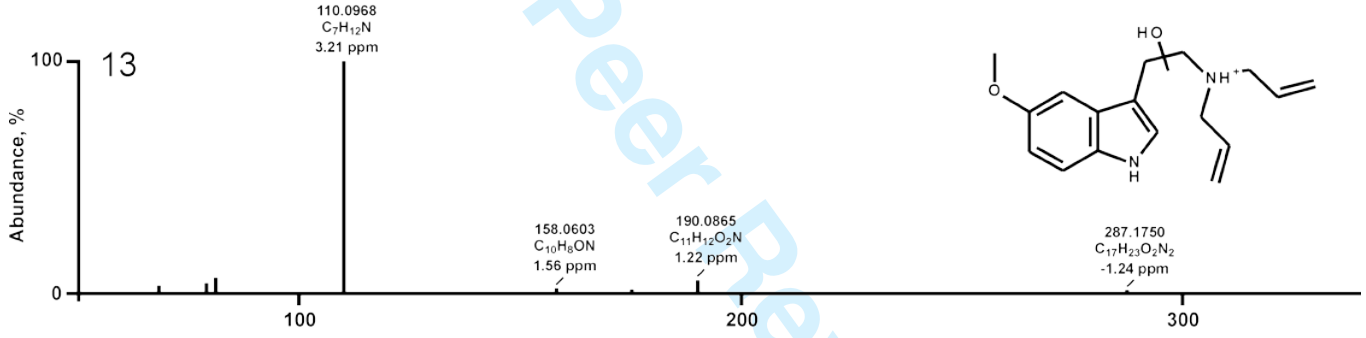

5-MeO-DALT-M (HO-alkyl-); RT 3.9

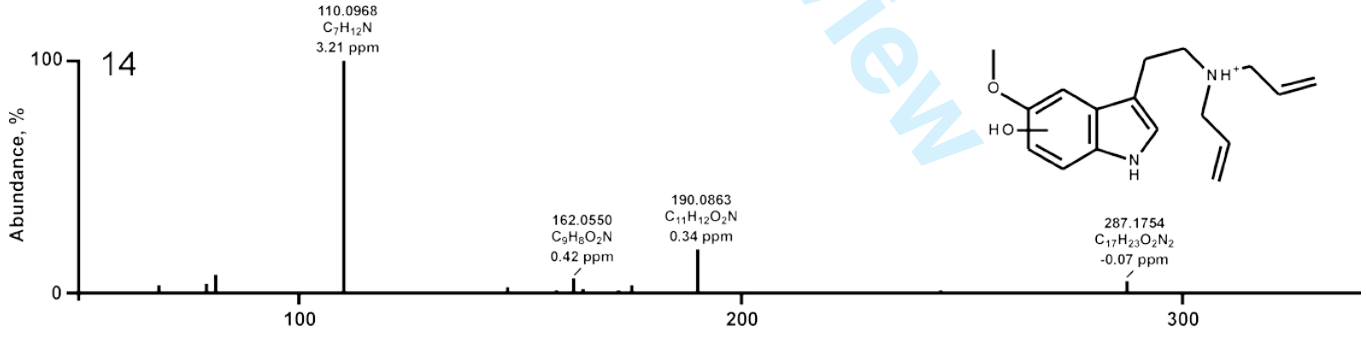

5-MeO-DALT-M (HO-aryl-); RT 4.1

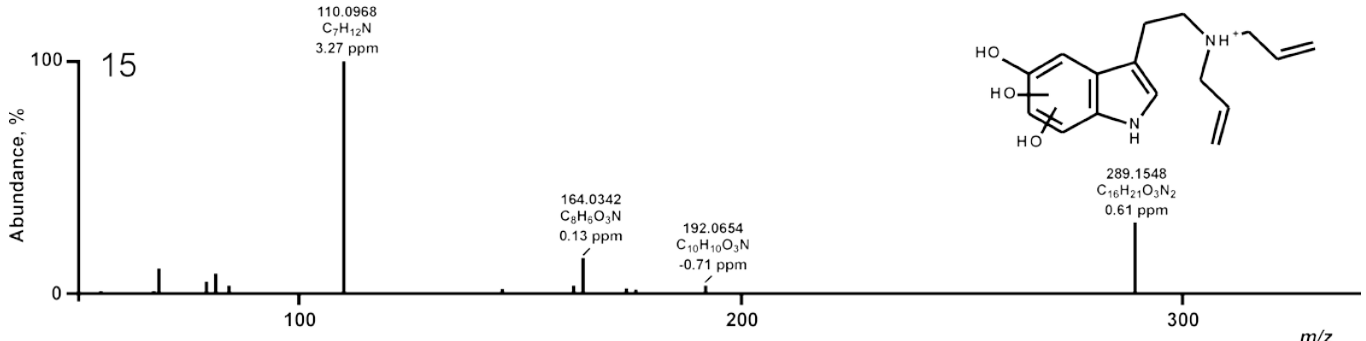

5-MeO-DALT-M (*O*-demethyl-di-HO-aryl-); RT 3.0

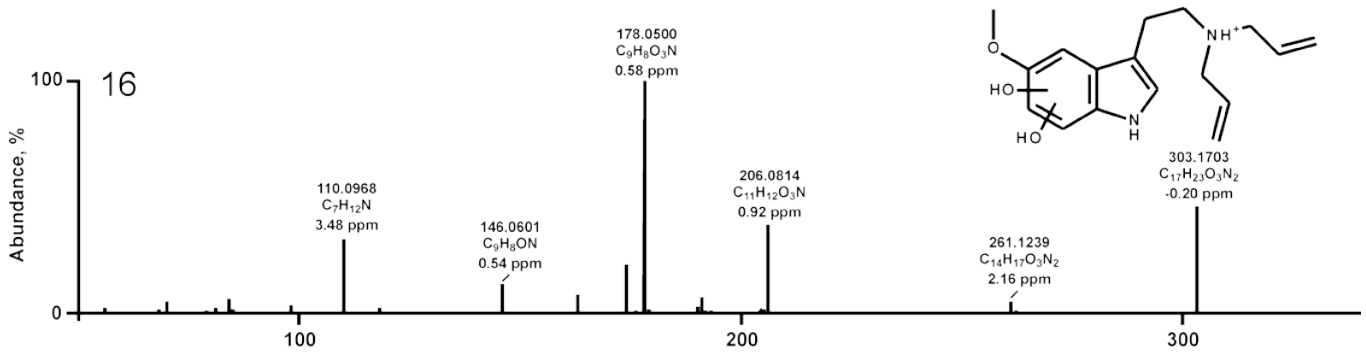

5-MeO-DALT-M (di-HO-aryl-) isomer 1; RT 4.0

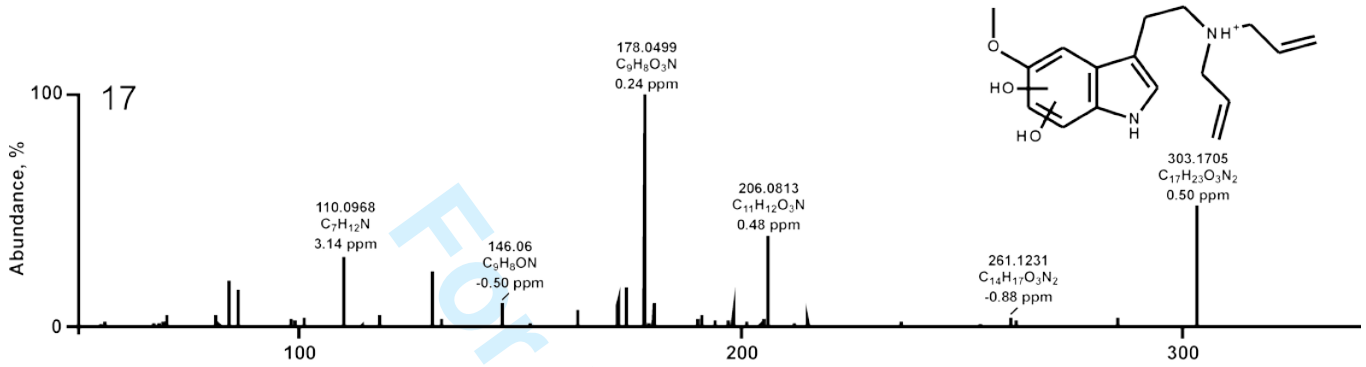

5-MeO-DALT-M (di-HO-aryl-) isomer 2; RT 4.2

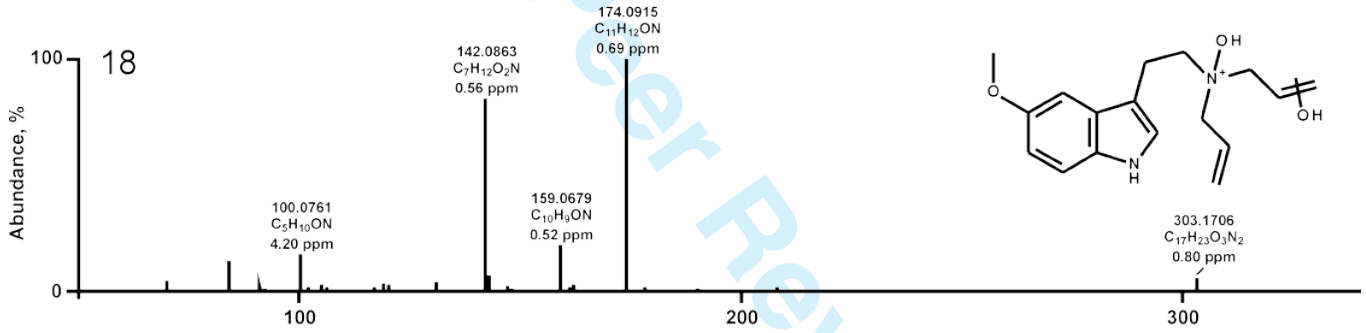

5-MeO-DALT-M (*N*-oxide-HO-alkyl-); RT 4.4

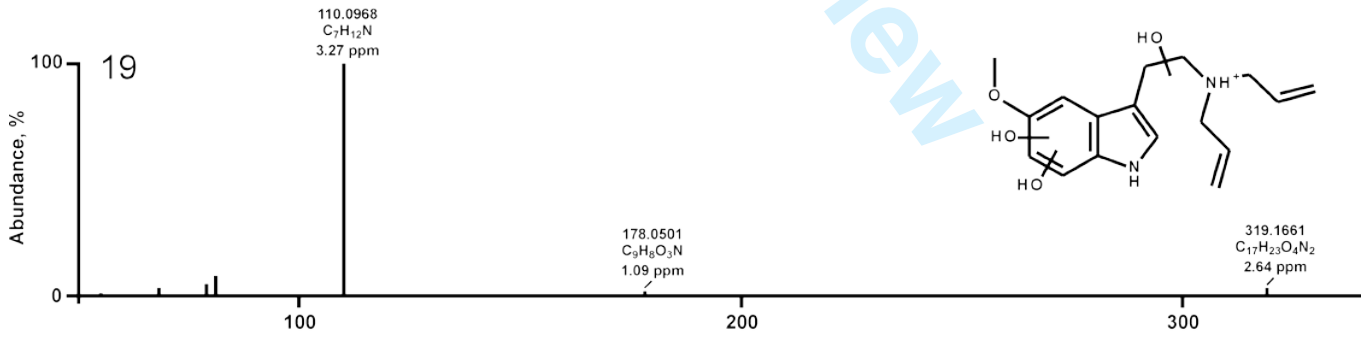

1,74 5-MeO-DALT-M (HO-alkyl-di-OH-aryl-); RT 3.3

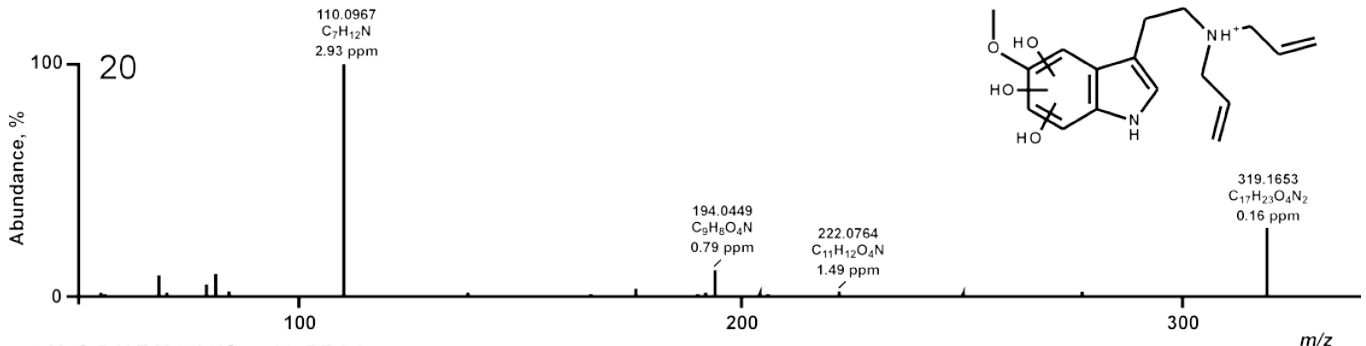

5-MeO-DALT-M (tri-HO-aryl-); RT 3.6

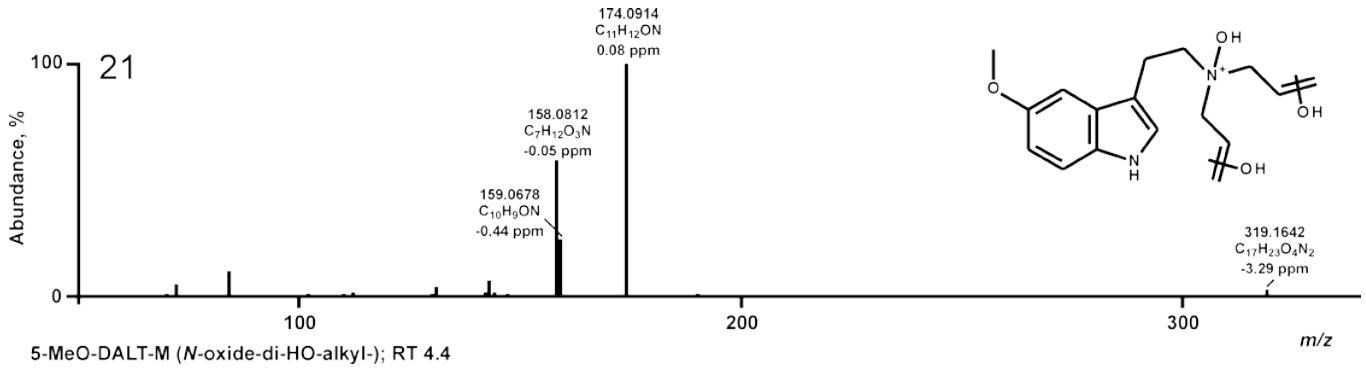

Fig. S2 LC-HR-MS/MS spectra of 5-MeO-DALT and its phase I metabolites arranged according to their precursor values, proposed chemical structures, accurate masses, calculated elemental formulas, and mass error values in parts per million (ppm) rounded to two decimals

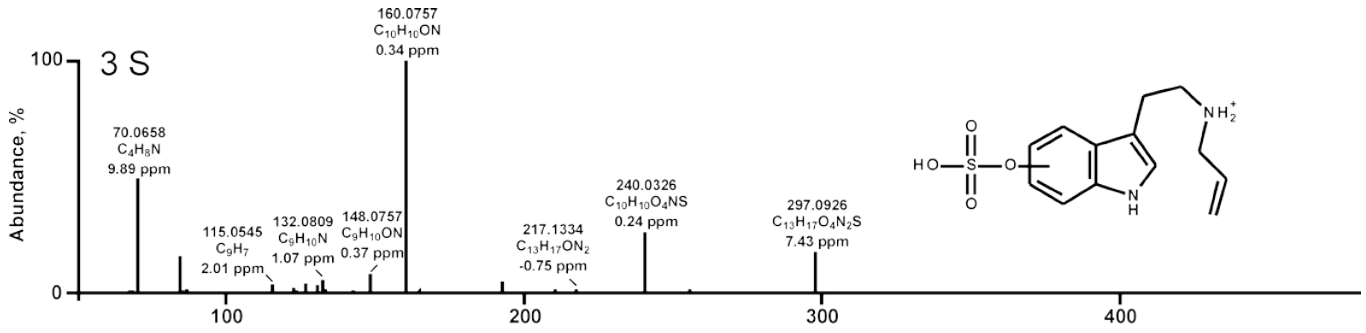

DALT-M (*N*-dealkyl-HO-aryl-sulfate) isomer 1; RT 3.4

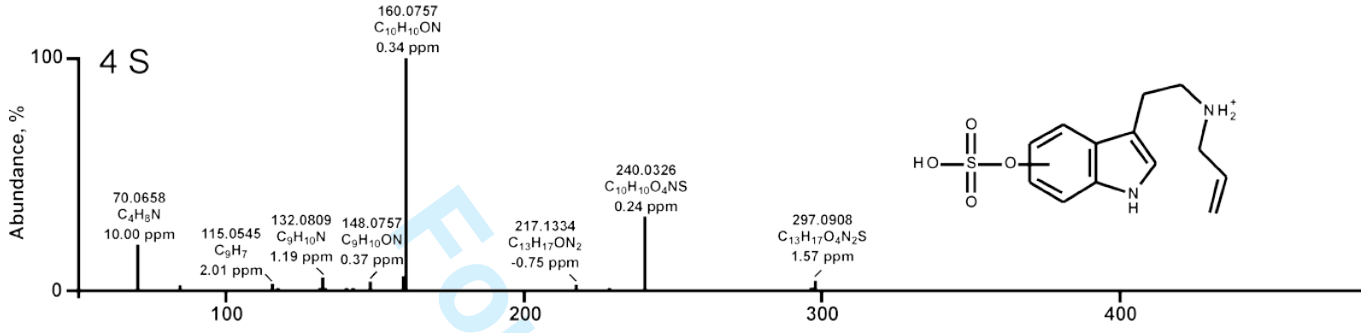

DALT-M (*N*-dealkyl-HO-aryl-sulfate) isomer 2; RT 3.8

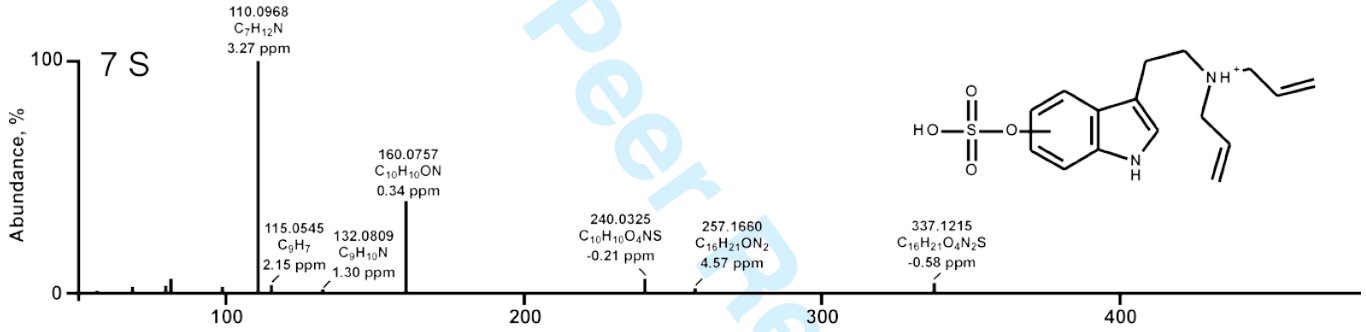

DALT-M (HO-aryl-sulfate) isomer 1; RT 4.0

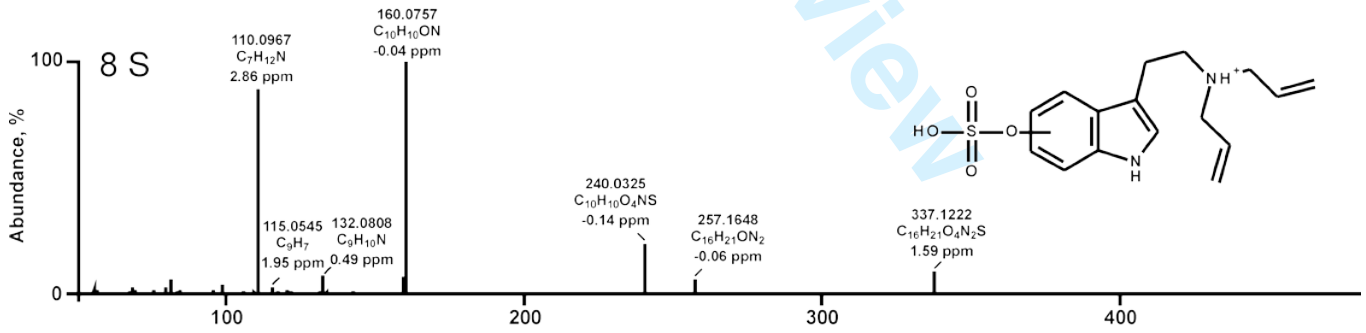

DALT-M (HO-aryl-sulfate) isomer 2; RT 4.4

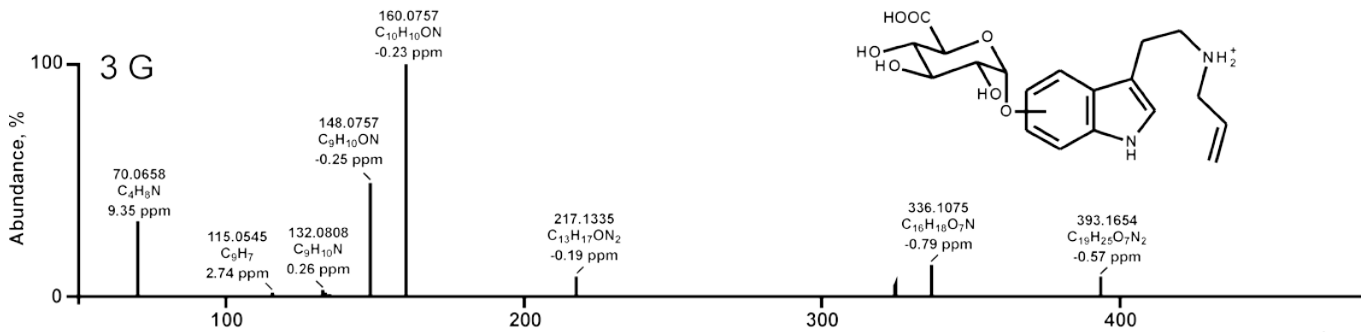

DALT-M (*N*-dealkyl-HO-aryl-glucuronide) isomer 1; RT 2.7

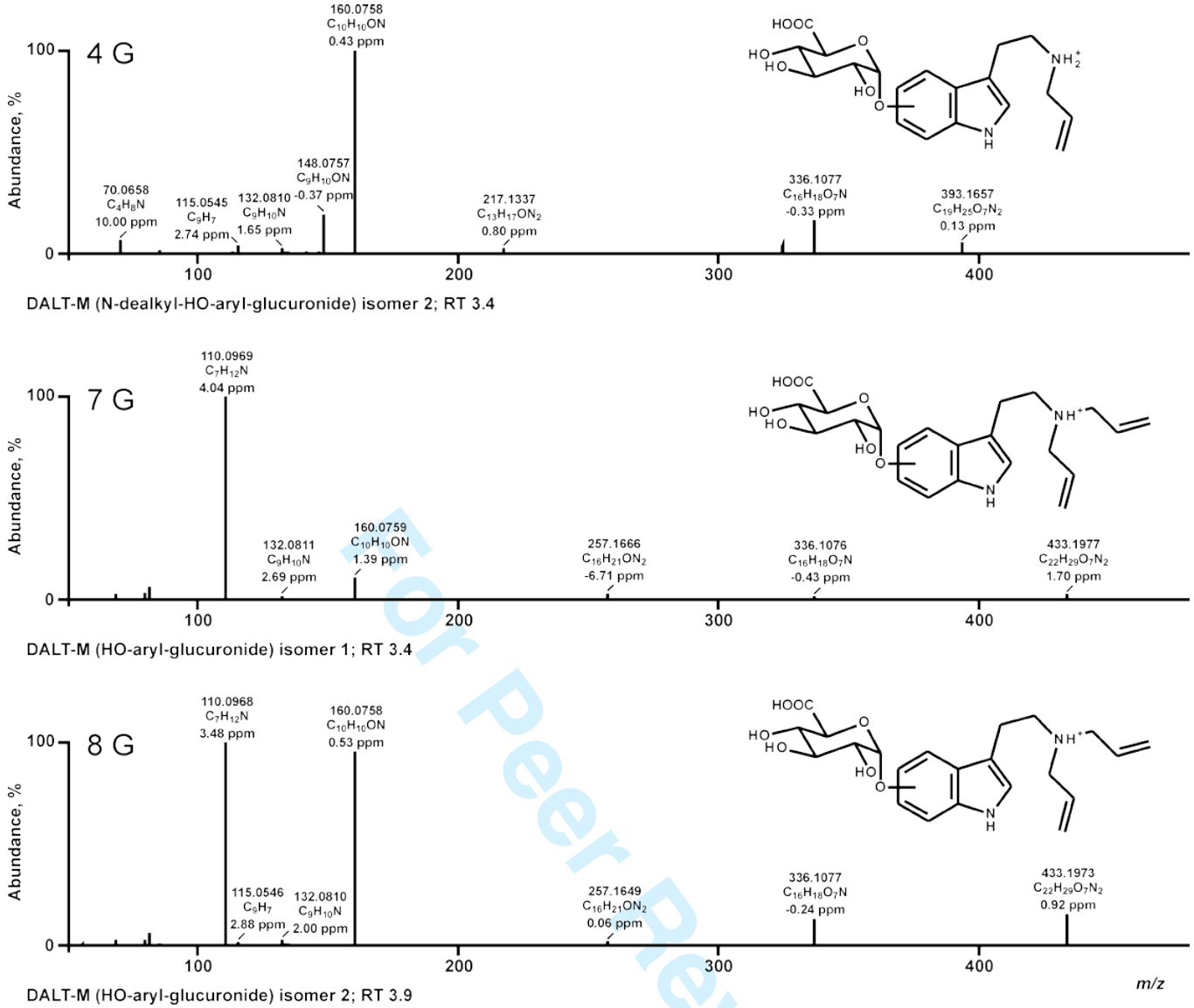

Fig. S3 LC-HR-MS/MS spectra of DALT phase II metabolites arranged according to their precursor values, proposed chemical structures, accurate masses, calculated elemental formulas, and mass error values in parts per million (ppm) rounded to two decimals

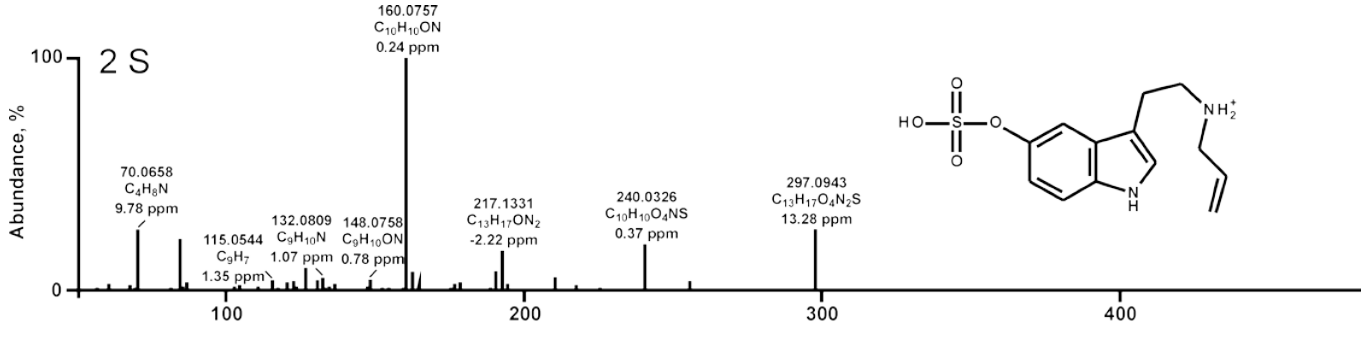

5-MeO-DALT-M (*O*-demethyl-*N*-dealkyl-sulfate); RT 3.3

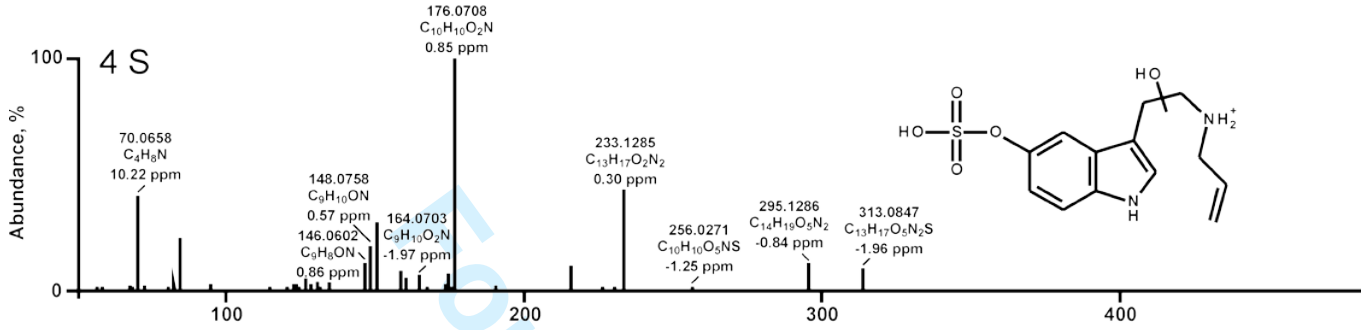

5-MeO-DALT-M (*O*-demethyl-*N*-dealkyl-HO-alkyl-sulfate); RT 2.7

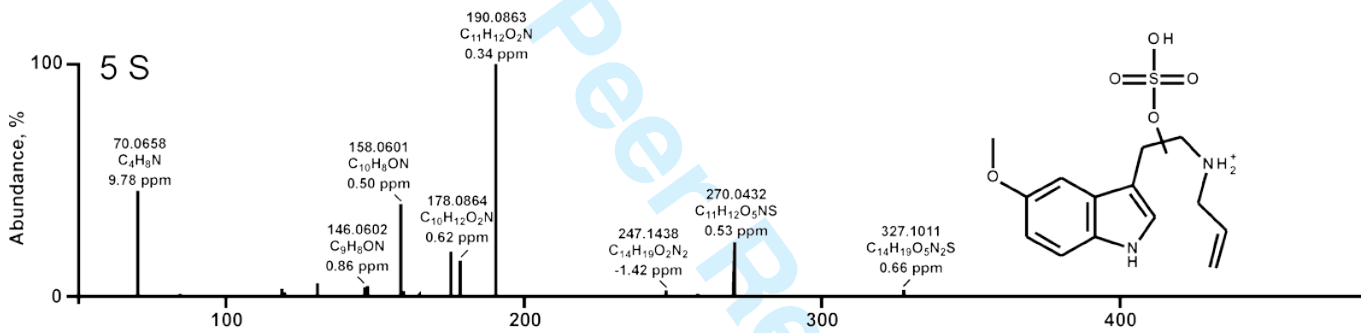

5-MeO-DALT-M (*N*-dealkyl-HO-alkyl-sulfate); RT 3.4

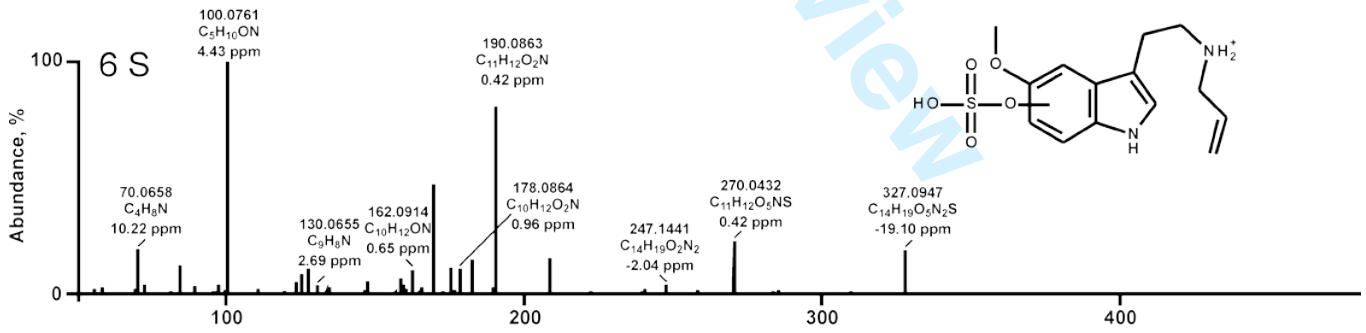

5-MeO-DALT-M (*N*-dealkyl-HO-aryl-sulfate); RT 4.0

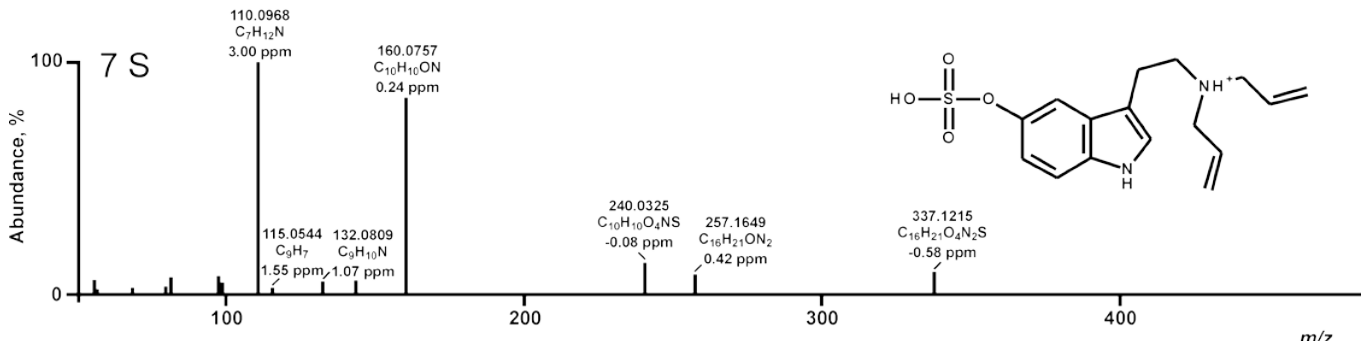

5-MeO-DALT-M (*O*-demethyl-sulfate); RT 3.9

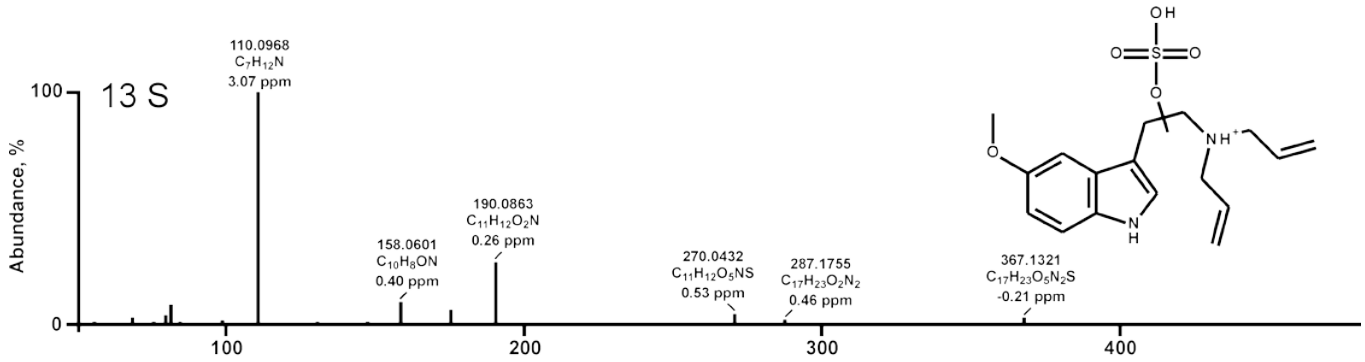

5-MeO-DALT-M (HO-alkyl-sulfate); RT 4.0

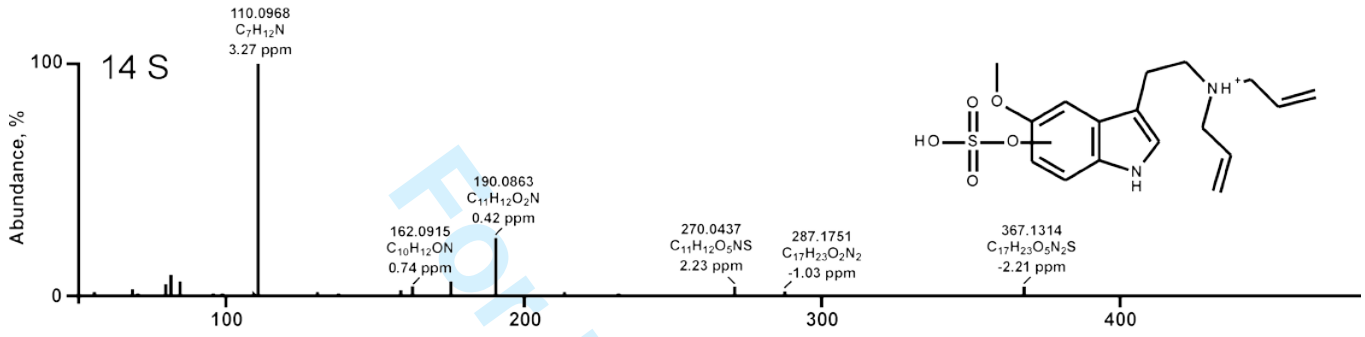

5-MeO-DALT-M (HO-aryl-sulfate); RT 4.1

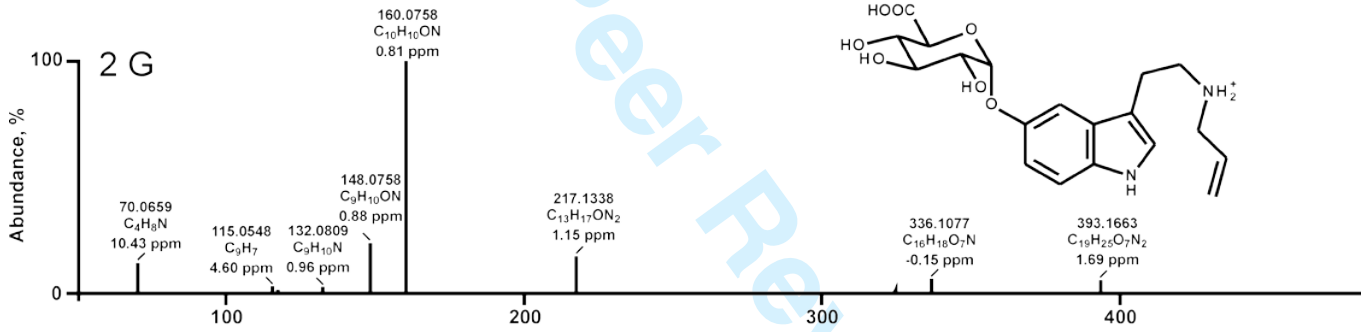

5-MeO-DALT-M (*O*-demethyl-*N*-dealkyl-glucuronide); RT 2.7

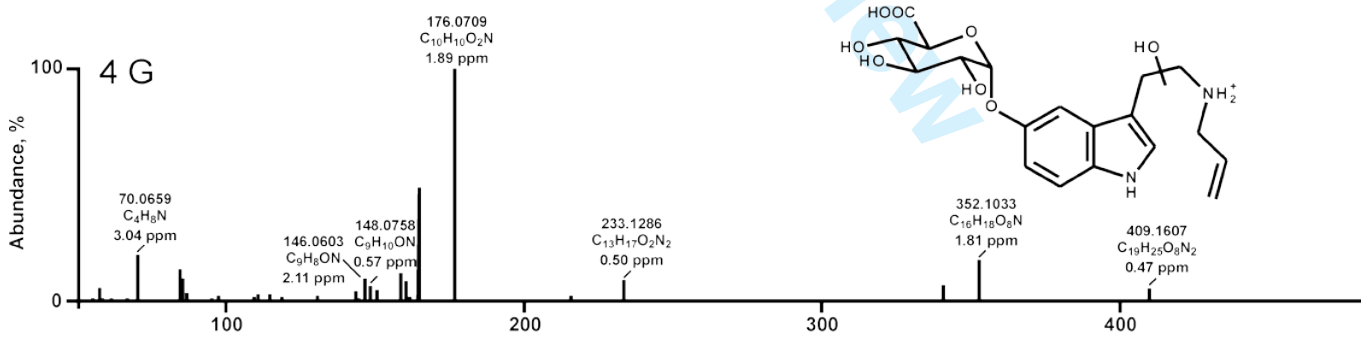

5-MeO-DALT-M (*O*-demethyl-*N*-dealkyl-HO-alkyl-glucuronide); RT 2.7

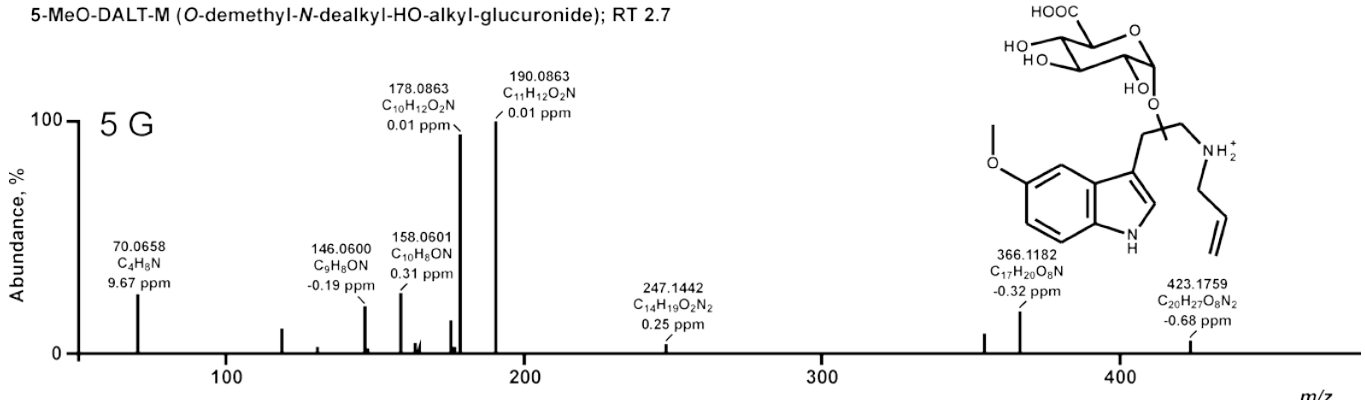

5-MeO-DALT-M (*N*-dealkyl-HO-alkyl-glucuronide); RT 3.0

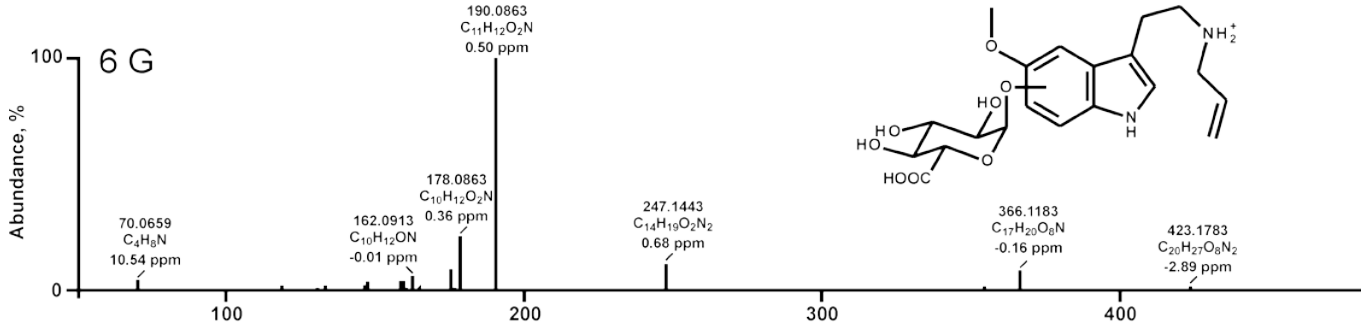

5-MeO-DALT-M (*N*-dealkyl-HO-aryl-glucuronide); RT 3.5

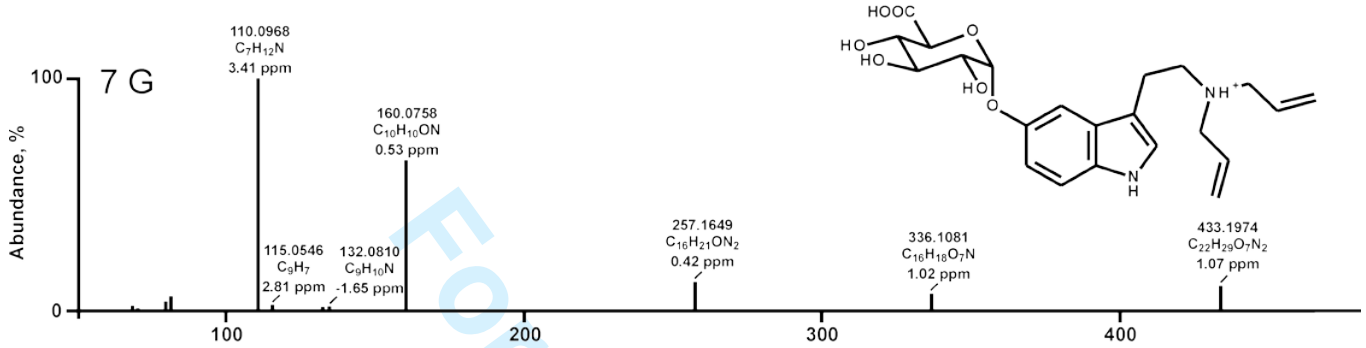

5-MeO-DALT-M (*O*-demethyl-glucuronide); RT 3.3

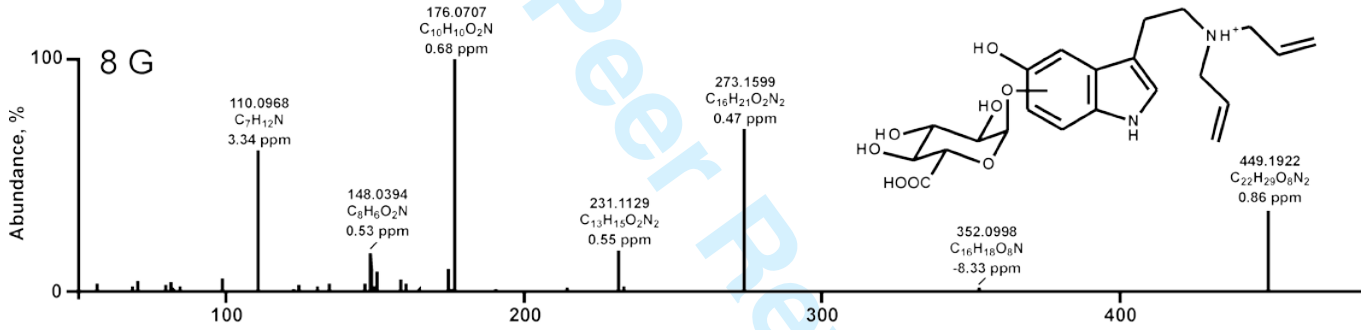

5-MeO-DALT-M (*O*-demethyl-HO-aryl-glucuronide); RT 2.7

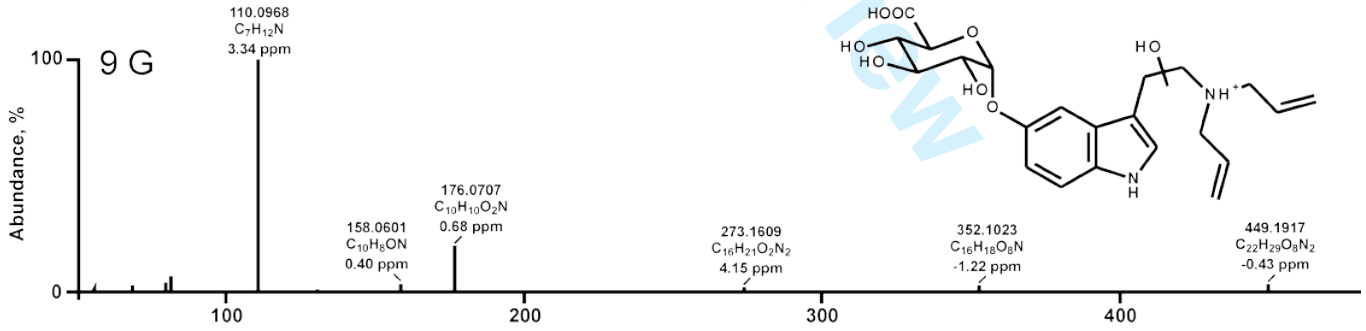

5-MeO-DALT-M (*O*-demethyl-HO-alkyl-glucuronide); RT 3.4

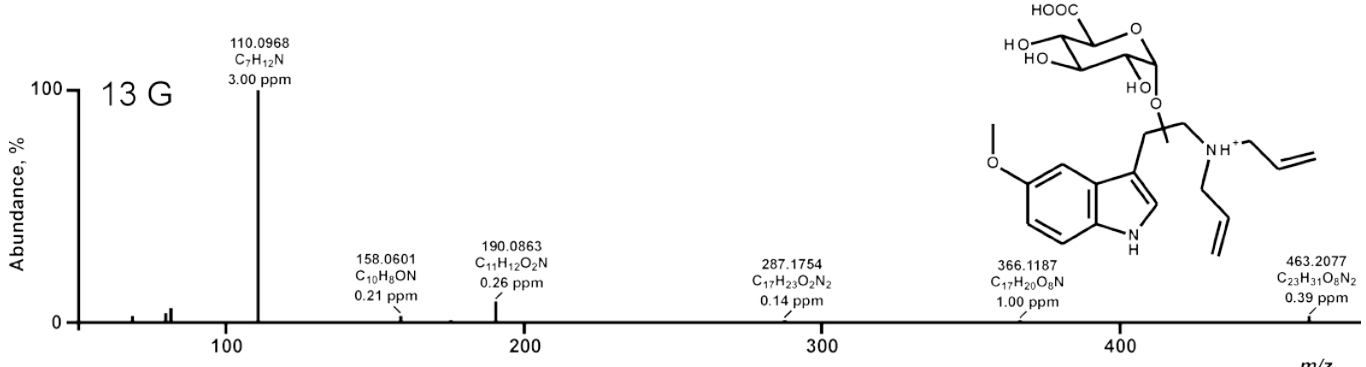

5-MeO-DALT-M (HO-alkyl-glucuronide); RT 3.6

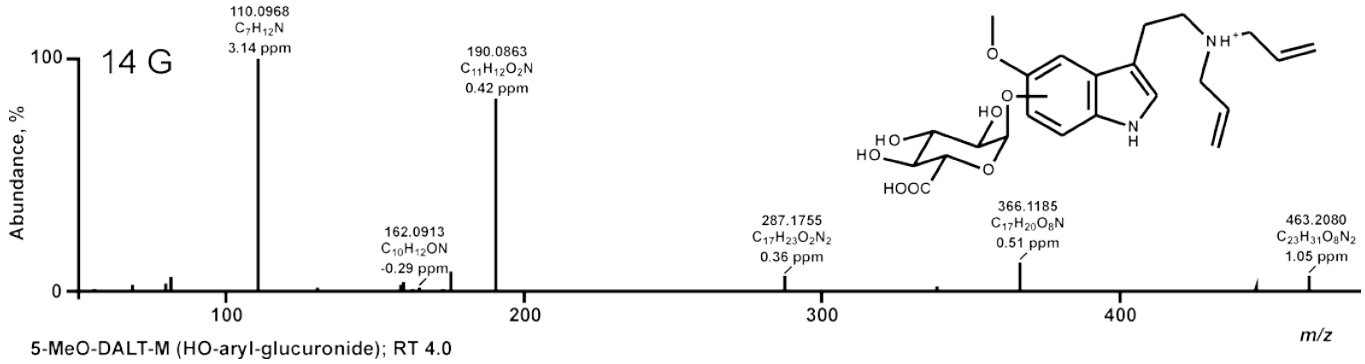

Fig. S4 LC-HR-MS/MS spectra of 5-MeO-DALT phase II metabolites arranged according to their precursor values, proposed chemical structures, accurate masses, calculated elemental formulas, and mass error values in parts per million (ppm) rounded to two decimals